

# The First GECAM Observation Results on Terrestrial Gamma-ray Flashes and Terrestrial Electron Beams

YI ZHAO<sup>1</sup>, Jia Cong Liu<sup>2</sup>, Shaolin Xiong<sup>3</sup>, Wangchen Xue<sup>2</sup>, Qibin Yi<sup>2</sup>, Gaopeng Lu<sup>4</sup>, Wei Xu<sup>5</sup>, Fanchao Lyu<sup>6</sup>, Jianchao Sun<sup>2</sup>, Wenxi Peng<sup>2</sup>, Chao Zheng<sup>2</sup>, Yanqiu Zhang<sup>2</sup>, Ce Cai<sup>7</sup>, Shuo Xiao<sup>8</sup>, Sheng-Lun Xie<sup>9</sup>, Chenwei Wang<sup>2</sup>, Wenjun Tan<sup>2</sup>, Zhenghua An<sup>3</sup>, gang chen<sup>2</sup>, yanqi du<sup>10</sup>, yue huang<sup>2</sup>, min gao<sup>2</sup>, ke gong<sup>2</sup>, dongya guo<sup>2</sup>, jianjian he<sup>2</sup>, bing li<sup>2</sup>, Gang Li<sup>11</sup>, Xinqiao Li<sup>3</sup>, xiaobo li<sup>2</sup>, liang jing<sup>10</sup>, Xiaohua Liang<sup>3</sup>, yaqing liu<sup>2</sup>, xiang ma<sup>2</sup>, rui qiao<sup>2</sup>, liming song<sup>2</sup>, xinying song<sup>2</sup>, xilei sun<sup>2</sup>, jin wang<sup>2</sup>, jinzhou wang<sup>2</sup>, Ping Wang<sup>12</sup>, Xiangyang Wen<sup>12</sup>, hong wu<sup>10</sup>, Yanbing Xu<sup>3</sup>, sheng yang<sup>2</sup>, boxin zhang<sup>2</sup>, Da Li Zhang<sup>13</sup>, fan zhang<sup>2</sup>, peng zhang<sup>14</sup>, hongmei zhang<sup>2</sup>, zhen zhang<sup>2</sup>, Xiaoyun Zhao<sup>3</sup>, shijie zheng<sup>2</sup>, keke zhang<sup>15</sup>, xingbo han<sup>15</sup>, haiyan wu<sup>16</sup>, tai hu<sup>16</sup>, hao geng<sup>16</sup>, Hongbo Zhang<sup>17</sup>, fangjun lu<sup>13</sup>, shuangnan zhang<sup>13</sup>, and heng yu<sup>1</sup>

<sup>1</sup>Beijing Normal University

<sup>2</sup>Key Laboratory of Particle Astrophysics, Institute of High Energy Physics, Chinese Academy of Sciences

<sup>3</sup>Institute of High Energy Physics

<sup>4</sup>School of Earth and Space Sciences, University of Science and Technology of China

<sup>5</sup>Wuhan University

<sup>6</sup>Nanjing Joint Institute for Atmospheric Sciences

<sup>7</sup>College of Physics and Hebei Key Laboratory of Photophysics Research and Application, Hebei Normal University

<sup>8</sup>School of Physics and Electronic Science, Guizhou Normal University

<sup>9</sup>Institute of Astrophysics, Central China Normal University

<sup>10</sup>School of Computing and Artificial Intelligence, Southwest Jiaotong University

<sup>11</sup>IHEP,CAS

<sup>12</sup>institute of high energy physics

<sup>13</sup>Institute of High Energy Physics, Chinese Academy of Sciences

<sup>14</sup>College of Electronic and Information Engineering, Tongji University

<sup>15</sup>Innovation Academy for Microsatellites of Chinese Academy of Sciences

<sup>16</sup>National Space Science Center, Chinese Academy of Sciences

<sup>17</sup>Institute of Atmospheric Physics, Chinese Academy of Sciences

December 22, 2022

## Abstract

Gravitational wave high-energy Electromagnetic Counterpart All-sky Monitor (GECAM) is a space-borne instrument dedicated to monitoring high-energy transients, therinto Terrestrial Gamma-ray Flashes (TGFs) and Terrestrial Electron Beams (TEBs). We propose a TGF/TEB search algorithm, with which 147 bright TGFs and 4 TEBs are identified during an effective observation time of  $\sim 9$  months. We show that, with gamma-ray and charged particle detectors, GECAM can effectively identify and

distinguish TGFs and TEBs, and measure their temporal and spectral properties in detail. Moreover, we find an interesting TEB consisting of two pulses with a separation of  $\sim 150$  ms, which is expected to originate from a lightning process near the geomagnetic footprint. We also find that the GECAM TGF's lightning-association ratio is  $\sim 80\%$  in the east Asia region using the GLD360 lightning network, which is significantly higher than previous observations.

# The First GECAM Observation Results on Terrestrial Gamma-ray Flashes and Terrestrial Electron Beams

Y. Zhao<sup>1,2</sup>, J. C. Liu<sup>2,3</sup>, S. L. Xiong<sup>2</sup>, W. C. Xue<sup>2,3</sup>, Q. B. Yi<sup>4,2</sup>, G. P. Lu<sup>5</sup>, W. Xu<sup>6</sup>, F. C. Lyu<sup>7</sup>, J. C. Sun<sup>2</sup>, W. X. Peng<sup>2</sup>, C. Zheng<sup>2,3</sup>, Y. Q. Zhang<sup>2,3</sup>, C. Cai<sup>8</sup>, S. Xiao<sup>9,10</sup>, S. L. Xie<sup>11</sup>, C. W. Wang<sup>2,3</sup>, W. J. Tan<sup>2,3</sup>, Z. H. An<sup>2</sup>, G. Chen<sup>2</sup>, Y. Q. Du<sup>12,2</sup>, Y. Huang<sup>2</sup>, M. Gao<sup>2</sup>, K. Gong<sup>2</sup>, D. Y. Guo<sup>2</sup>, J. J. He<sup>2</sup>, B. Li<sup>2</sup>, G. Li<sup>2</sup>, X. Q. Li<sup>2</sup>, X. B. Li<sup>2</sup>, J. Liang<sup>12,2</sup>, X. H. Liang<sup>2</sup>, Y. Q. Liu<sup>2</sup>, X. Ma<sup>2</sup>, R. Qiao<sup>2</sup>, L. M. Song<sup>2</sup>, X. Y. Song<sup>2</sup>, X. L. Sun<sup>2</sup>, J. Wang<sup>2</sup>, J. Z. Wang<sup>2</sup>, P. Wang<sup>2</sup>, X. Y. Wen<sup>2</sup>, H. Wu<sup>12,2</sup>, Y. B. Xu<sup>2</sup>, S. Yang<sup>2</sup>, B. X. Zhang<sup>2</sup>, D. L. Zhang<sup>2</sup>, F. Zhang<sup>2</sup>, P. Zhang<sup>13,2</sup>, H. M. Zhang<sup>2</sup>, Z. Zhang<sup>2</sup>, X. Y. Zhao<sup>2</sup>, S. J. Zheng<sup>2</sup>, K. K. Zhang<sup>14</sup>, X. B. Han<sup>14</sup>, H. Y. Wu<sup>15</sup>, T. Hu<sup>15</sup>, H. Geng<sup>15</sup>, F. J. Lu<sup>2</sup>, S. N. Zhang<sup>2</sup>, H. Yu<sup>1</sup>

<sup>1</sup>Department of Astronomy, Beijing Normal University, Beijing 100875, Beijing, China

<sup>2</sup>Key Laboratory of Particle Astrophysics, Institute of High Energy Physics, Chinese Academy of Sciences, Beijing 100049, Beijing, China

<sup>3</sup>University of Chinese Academy of Sciences, Beijing 100049, Beijing, China

<sup>4</sup>School of Physics and Optoelectronics, Xiangtan University, Xiangtan 411105, Hunan, China

<sup>5</sup>School of Earth and Space Sciences, University of Science and Technology of China, Hefei 230026, Anhui, China

<sup>6</sup>Electronic Information School, Wuhan University, Wuhan 430072, Hubei, China

<sup>7</sup>Key Laboratory of Transportation Meteorology of China Meteorological Administration, Nanjing Joint Institute for Atmospheric Sciences, Nanjing 210000, Jiangsu China

<sup>8</sup>College of Physics and Hebei Key Laboratory of Photophysics Research and Application, Hebei Normal University, Shijiazhuang, Hebei 050024, China

<sup>9</sup>Guizhou Provincial Key Laboratory of Radio Astronomy and Data Processing, Guizhou Normal University, Guiyang 550001, GuiZhou, China

<sup>10</sup>School of Physics and Electronic Science, Guizhou Normal University, Guiyang 550001, GuiZhou, China

<sup>11</sup>Institute of Astrophysics, Central China Normal University, Wuhan 430079, HuBei, China

<sup>12</sup>School of Computing and Artificial Intelligence, Southwest Jiaotong University, Chengdu 611756, SiChuan, China

<sup>13</sup>College of Electronic and Information Engineering, Tongji University, Shanghai 201804, Shanghai, China

<sup>14</sup>Innovation Academy for Microsatellites of Chinese Academy of Sciences, Shanghai 201304, Shanghai, China

<sup>15</sup>National Space Science Center, Chinese Academy of Sciences, Beijing 100190, Beijing, China

## Key Points:

- GECAM can well classify and distinguish TGF/TEB, and reveal their fine temporal and spectral features, e.g. short spikes down to 10 ms.
- GECAM discovered an interesting two-peaked TEB which is probably from a lightning process near the geomagnetic footprint.
- TGF-lightning association rate between GECAM and GLD360 in east Asia is found to be  $\sim 80\%$ , notably higher than previous reports.

---

Corresponding author: S. L. Xiong, [xiongs1@ihep.ac.cn](mailto:xiongs1@ihep.ac.cn)

**Abstract**

Gravitational wave high-energy Electromagnetic Counterpart All-sky Monitor (GECAM) is a space-borne instrument dedicated to monitoring high-energy transients, therewith Terrestrial Gamma-ray Flashes (TGFs) and Terrestrial Electron Beams (TEBs). We propose a TGF/TEB search algorithm, with which 147 bright TGFs and 4 TEBs are identified during an effective observation time of  $\sim 9$  months. We show that, with gamma-ray and charged particle detectors, GECAM can effectively identify and distinguish TGFs and TEBs, and measure their temporal and spectral properties in detail. Moreover, we find an interesting TEB consisting of two pulses with a separation of  $\sim 150$  ms, which is expected to originate from a lightning process near the geomagnetic footprint. We also find that the GECAM TGF's lightning-association ratio is  $\sim 80\%$  in the east Asia region using the GLD360 lightning network, which is significantly higher than previous observations.

**Plain Language Summary**

Terrestrial gamma-ray flashes (TGFs) and Terrestrial Electron Beams (TEBs) are one of the most energetic radioactive phenomena in the atmosphere of the Earth. They reflect a natural particle accelerator that can boost electrons up to at least several tens of mega electron volts (MeV). With novel detection technologies, GECAM is a new powerful instrument to observe TGFs and TEBs, as well as study their properties. For example, it is difficult for most space-borne high-energy instruments to distinguish between TGFs and TEBs. With the joint observation of gamma-ray and charged particle detectors, GECAM can effectively identify TGFs and TEBs. GECAM can also reveal fine features in the light curves and spectra of these bursts. Interestingly, GECAM discovered the first, as far as we are aware of, TEB which consists of two pulses with a separation time of about 150 ms. Unlike the case in previous TEBs, the second pulse is not the return peak but has the same origin as the first one.

**1 Introduction**

Terrestrial Gamma-ray Flashes (TGFs) are submillisecond intense bursts of  $\gamma$ -rays with energies up to several tens of MeV (Briggs et al., 2010; Marisaldi et al., 2010, 2019), which was serendipitously discovered by the Burst and Transient Source Experiment (BATSE) aboard Compton Gamma-ray Observatory (CGRO) in 1991 (Fishman et al., 1994). Since then, TGFs have been routinely observed by space-borne instruments, such as BeppoSAX (Ursi et al., 2017), RHESSI (Grefenstette et al., 2009), AGILE (Marisaldi et al., 2010), *Fermi*/GBM (Roberts et al., 2018) and ASIM (Østgaard et al., 2019) during last three decades. Occasionally, TGFs can also be observed by ground instruments (Dwyer et al., 2012), however, the strong absorption of gamma-rays in the air makes the detection very difficult.

TGFs observed by these space-borne instruments are widely believed to be produced through the initial upward leader of positive Intracloud (+IC) lightning (Lu et al., 2010, 2011). They are the results of relativistic electrons that produce hard X/ $\gamma$ -rays through the bremsstrahlung process. These electrons are accelerated in a very high electric field by the runaway process (Wilson, 1925) and multiplied by many orders of magnitude through the Relativistic Runaway Electron Avalanche process (Gurevich et al., 1992; Dwyer & Smith, 2005). Two main models were proposed to explain the production of TGFs. One is the lightning leader model, which involves the acceleration of free electrons under the localized electric field in front of lightning leader tips (Moss et al., 2006; Dwyer, 2010; Celestin & Pasko, 2011; Celestin et al., 2013). The other one is the relativistic feedback model (RFD) (Dwyer, 2003; Dwyer, 2008, 2012; Liu & Dwyer, 2013), which considers the feedback processes from positrons and photons in a large-scale electric field region.

92 However, the specific mechanism to produce  $\sim 10^{17}$  to  $10^{19}$  electrons is still an open ques-  
93 tion (Chanrion & Neubert, 2010; Xu et al., 2012, 2015; Skeltved et al., 2017).

94 By interacting with the atmosphere during the propagation, the TGF photons can  
95 produce secondary electrons and positrons. Then they will move along the Earth's mag-  
96 netic field line, forming Terrestrial Electron Beams (TEBs) (Dwyer et al., 2008), which  
97 could be observed by some TGF-detecting instruments (Xiong et al., 2012; Lindanger  
98 et al., 2020; Sarria et al., 2021).

99 In this study, the data of Gravitational-wave high-energy Electromagnetic Coun-  
100 terpart All-sky Monitor (GECAM) (Li et al., 2022) are utilized for TGFs and TEBs re-  
101 search. GECAM is a space-based instrument dedicated to the observation of gamma-  
102 ray electromagnetic counterparts of the Gravitational Waves (Goldstein et al., 2017) and  
103 Fast Radio Bursts (Lorimer et al., 2007), as well as other high-energy astrophysical and  
104 terrestrial transient sources, such as Gamma-ray Bursts (GRBs) (Klebesadel et al., 1973),  
105 Soft Gamma-ray Repeaters (SGRs) (Woods & Thompson, 2004), solar flares, TGFs and  
106 TEBs.

107

## 2 Instrument and Search Algorithm

Since the launch in December 2020, GECAM has been operating in low earth orbit (600 km altitude and 29° inclination angle) (Han et al., 2020). GECAM consists of twin micro-satellites (i.e. GECAM-A and GECAM-B) and each of them comprises 25 Gamma-ray Detectors (GRDs) (An et al., 2022) and 8 Charged Particle Detectors (CPDs) (Xu et al., 2022). It should be noted that only GECAM-B data are utilized in this study because GECAM-A has not been able to observe yet (Li et al., 2022).

With  $\text{LaBr}_3$  crystals read out by silicon photomultiplier (SiPM) arrays, GRDs can detect high-energy photons in a broad energy range of  $\sim 15$  keV to  $\sim 5$  MeV (Zhang et al., 2022). CPDs are designed to detect the charged particles from  $\sim 100$  keV to  $\sim 5$  MeV. The joint observation of GRDs and CPDs can distinguish between gamma-rays and charged particle bursts, such as TGFs and TEBs (Zhao et al., 2021).

To detect those extremely short and bright bursts, e.g. TGFs and TEBs, a dedicated anti-saturation data acquisition system (DAQ) is designed for GECAM. The data buffer in DAQ can accommodate up to 4092 and 1020 counts for the high-gain and low-gain of each GRD, respectively. Since there are usually several hundred counts registered for a bright TGF, the GECAM DAQ can guarantee to transfer and save almost all TGFs photons that are recorded by detectors (Liu et al., 2021).

For GRD, the dead time is 4  $\mu\text{s}$  for normal events and  $> 69$   $\mu\text{s}$  for overflow events (i.e. events with higher energy deposition than the maximum measurable energy). Each GRD detector has two read-out channels: high-gain channel ( $\sim 15$  keV to  $\sim 300$  keV) and low-gain channel ( $\sim 300$  keV to  $\sim 5$  MeV) (Liu et al., 2021). The design, performance, and other information about GECAM have been reported by Li et al. (2022); An et al. (2022); Xu et al. (2022).

The considerable number of GRD detectors is helpful to locate the source region of TGFs. We have proposed a dedicated localization method for all-sky monitor which can be used for extremely short-duration TGFs (Zhao et al. 2022a). Despite the low counting statistics of TGFs, GECAM can still locate TGFs (Zhao et al. 2022b).

As the main contamination source for TGFs, cosmic-ray events show very similar patterns in data as TGFs, but with an even shorter duration. Thanks to the high time resolution of GECAM, i.e. 100 ns (Xiao et al., 2022), GECAM can effectively distinguish between cosmic-ray events and TGFs. Indeed, a dedicated data product called Simultaneous Events is designed for GECAM. The Simultaneous Events Number (SimEvtNum) is defined as the number of events from different detectors registered in the same 300 ns time window (Xiao et al., 2022). As the SimEvtNum increases, the probability of these events caused by cosmic-rays surges. Here a relatively loose criterion (SimEvtNum  $> 13$ ) is adopted for basic data selection.

To unveil TGFs and TEBs in GECAM data, we developed a dedicated burst search algorithm, which is very different from normal burst search for gamma-ray bursts (Cai et al., 2021, 2022), because the TGF and TEB are so weak that only a few counts are registered in each detector, and both GRDs and CPDs are needed in the search. The event-by-event (EVT) data of GECAM GRDs and CPDs are used in this study. Only recommended normal events with SimEvtNum  $< 13$  are utilized. We divide 25 GRDs into four groups considering the neighboring position, and it turns out that there are 6 [7] GRDs for 3 [1] group(s). All 8 CPDs are treated as a single group.

Assuming the background follows the Poisson distribution, the probability that the counts are from background fluctuation can be calculated as,

$$P_{\text{group}}(S \geq S' | B) = 1 - \sum_{S=0}^{S=S'-1} \frac{B^S \cdot \exp(-B)}{S!}, \quad (1)$$

155 where  $S$  and  $S'$  are observed counts and threshold counts, respectively, for one group  
 156 in a time window,  $B$  is the estimated background for the time window calculated by the  
 157 average counts over  $T_{\text{rela}} \in [-5, -1]$  s and  $\in [+1, +5]$  s, where  $T_{\text{rela}}$  is the relative time with  
 158 respect to the end time of the time window.

159 For an individual searching bin, the joint probability of at least  $N'_{\text{trig}}$  group(s) out  
 160 of total group number  $M$  passing the trigger threshold for a single group  $P_{\text{group}}$  is,

$$P_{\text{bin}}(N_{\text{trig}} \geq N'_{\text{trig}}) = \sum_{N_{\text{trig}}=N'_{\text{trig}}}^{N_{\text{trig}}=M} C_M^{N_{\text{trig}}} \cdot (P_{\text{group}})^{N_{\text{trig}}} \cdot (1 - P_{\text{group}})^{M - N_{\text{trig}}}. \quad (2)$$

161 In this work, seven time scales are utilized to do searching. The widths of time scales  
 162 with the corresponding empirical threshold  $P_{\text{tot}}$  are: 50  $\mu\text{s}$  ( $5.0 \times 10^{-22}$ ), 100  $\mu\text{s}$  ( $2.0 \times$   
 163  $10^{-21}$ ), 250  $\mu\text{s}$  ( $1.3 \times 10^{-20}$ ), 500  $\mu\text{s}$  ( $5.0 \times 10^{-20}$ ), 1 ms ( $2.0 \times 10^{-19}$ ), 2 ms ( $8.0 \times 10^{-19}$ ),  
 164 4 ms ( $3.2 \times 10^{-18}$ ). All of them are used for TGF search while only the latter four are  
 165 for TEB search. It should be noted that these empirical criteria are relatively strict so  
 166 that only intense TGFs or TEBs could be identified.

167 By setting  $P_{\text{tot}} = P_{\text{bin}}$ , the group's trigger threshold ( $P_{\text{group,GRD}}$ ) can be obtained  
 168 for TGF with GRDs from the following equation (i.e.  $M = 4$ , and we set  $N'_{\text{trig,GRD}} =$   
 169 2),

$$P_{\text{tot,GRD}}(N_{\text{trig}} \geq 2) = 6 \cdot P_{\text{group,GRD}}^2 - 8 \cdot P_{\text{group,GRD}}^3 + 3 \cdot P_{\text{group,GRD}}^4, \quad (3)$$

170 and the trigger threshold from the following equation of TEB with CPDs ( $M = 1$ , and  
 171 we set  $N'_{\text{trig,CPD}} = 1$ ),

$$P_{\text{tot,CPD}} = P_{\text{group,CPD}}. \quad (4)$$

172 According to the empirical threshold above, the trigger threshold for each detector group  
 173 can be obtained for each searching window, e.g. for 100  $\mu\text{s}$ ,  $P_{\text{group,GRD}} = 1.8 \times 10^{-11}$   
 174 which corresponds to 6.6  $\sigma$  in standard Gaussian distribution.

175 For a candidate to be identified as a TGF/TEB, all criteria below must be met:

- 176 1. The trigger threshold (Equations 3 and 4) must be satisfied.
- 177 2. The candidate should not be SGR. It should be noticed that millisecond-duration  
 178 SGRs can be searched in the time scale of milliseconds with a much softer spec-  
 179 trum than TGFs.
- 180 3. Should not be caused by instrument effects, which are characterized by that there  
 181 is significant excess (Poisson significance  $> 6 \sigma$ ) registered in 2 to 3 GRDs while  
 182 no obvious signals (Poisson significance  $< 3 \sigma$ ) for most (i.e.  $> 21$ ) GRDs.
- 183 4. For filtering out cosmic-rays, the ratio of the simultaneous event ( $R_{\text{sim},7}^1$ ) should  
 184 be  $< 20\%$ .

---

<sup>1</sup>  $R_{\text{sim},7}$ : the total number of simultaneous events registered in  $> 7$  GRDs, divided by the total events number in the searching bin.

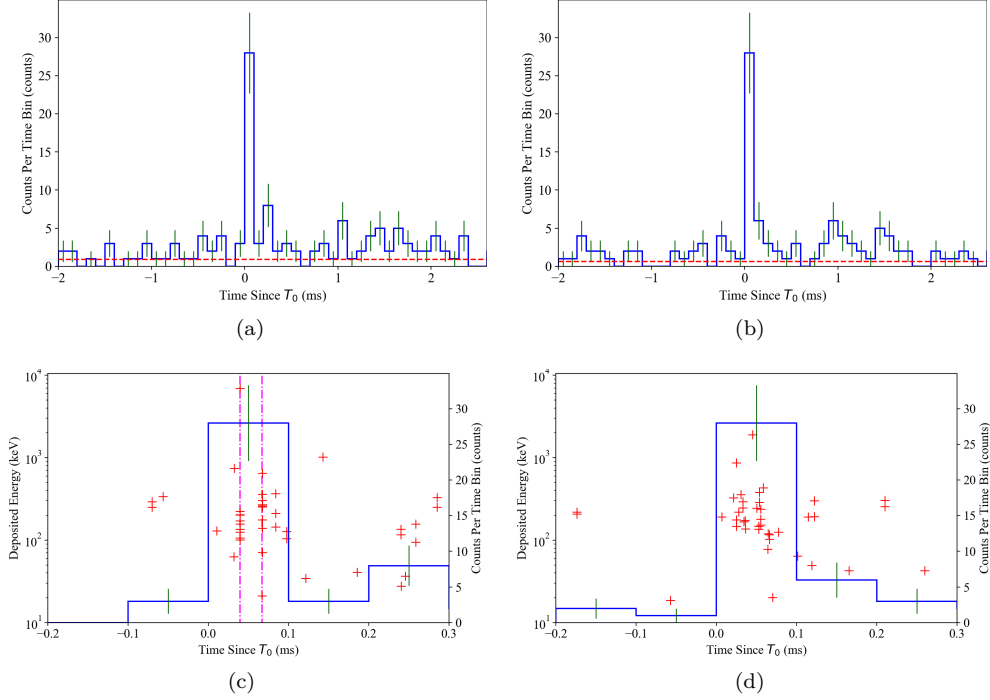


**Figure 1.** Illustration of distinguishing between cosmic-rays and TGFs by simultaneous events. (a) and (c): the light curve and time-energy scatter plot of a cosmic-ray event. (b) and (d): the light curve and time-energy scatter plot of a TGF. The dot-dashed lines show the time edge of simultaneous events registered in  $> 7$  GRDs within 300 ns. The horizontal and vertical scales are the same for the two events.

185  
186  
187  
188  
189  
190

For the identification of TEBs, more criteria are needed which will be described in Section 4. To further illustrate the capability of GECAM to identify cosmic-rays, a case is illustrated in Figure 1. The classification of the two excesses can not be distinguished well just according to the light curves. However, the cosmic-ray event (Figure 1a and 1c) has  $F_{\text{sim},7} = \frac{18}{28} \approx 64\%$ , while TGFs have no simultaneous events registered in  $> 7$  GRDs (Figure 1b and 1d).

### 3 GECAM TGFs

From December 10th, 2020 to August 31st, 2022, the effective observation time of GECAM-B is  $\sim 274.5$  days ( $\sim 0.75$  years). As shown in Figure 2, 147 bright TGFs are identified by our search algorithm, corresponding to a discovery rate of  $\sim 200$  TGFs/year or 0.54 TGFs/day. The Global Lightning Dataset (GLD360) is utilized to match lightning for GECAM TGFs in the time window of  $\pm 5$  ms corrected for the light propagation time and within the distance window of 800 km from GECAM nadirs. The GLD360 lightning-association ratio is  $\frac{34}{42} \approx 80\%$  in the east Asia region (EAR,  $77^\circ$  E– $138^\circ$  E,  $13^\circ$  S– $30^\circ$  N) which is  $\sim 2.5$  times of the results based on the data of the other spaceborne instruments and the World Wide Lightning Location Network (WWLLN) lightning ( $\sim 33\%$ ) (Roberts et al., 2018; Maiorana et al., 2020). The high lightning-association ratio may be attributed to two factors: (1) the detection efficiency of GLD360 is higher than the other lightning location network at least in EAR (Said et al., 2013; Poelman et al., 2013; Pohjola & Mäkelä, 2013), (2) the current GECAM TGF sample only contains bright ones, resulting from the very strict searching threshold. The sphere distance between the GECAM nadirs and the associated GLD360 lightning inside the EAR ranges from  $\sim 50$  km to 800 km, which is consistent with previous reports.

The statistical distribution of temporal, intensity and energy properties of this GECAM TGF sample are shown in Figure 3. The duration is calculated by the Bayesian Block (BB) algorithm (Scargle et al., 2013). Since the relatively strict threshold, faint TGFs are dropped from the current sample. Therefore, the GECAM TGF discovery rate would increase as we decrease the search threshold in the future. As shown in Figure 3c, TGF events with relatively shorter duration tend to have a harder spectrum and thus more high-energy electrons in the source region, which is in line with previous observations (Briggs et al., 2013). As shown in Figure 3d, the duration and CPD/GRD counts ratio is very effective to classify TGFs and TEBs (see Section 4).

In Figure 4, the light curves and time-energy scatter plots are illustrated for three multipeak, three bright, and two short TGFs. The fraction of multipeak TGFs is  $\frac{3}{147} \approx 2\%$ , which is consistent with that observed by the other instruments (Mezentsev et al., 2016; Lindanger et al., 2020). Since the upward leader channel of a lightning discharge would generally branch into several channels during propagation, it is widely accepted that the temporal structures may reflect the electric field distribution that the leaders have passed through. This effect is more pronounced in the multipeak or overlapping structures of TGFs.

It is worth noticing an interesting double-peaked TGF (Figure 4a) which is characterized by two  $\sim 100 \mu\text{s}$  pulses with very similar temporal and spectral structures. Two possible scenarios may explain this double-peaked TGF. For the first, it could be associated with two leader branches propagating in two distinct localized electric fields, which could be also responsible for the cases shown in Figure 4b to 4c. However, this double-peak TGF (Figure 4a) may require coincidences comparing to other TGFs in Figure 4b to 4c, i.e. two intracloud electric fields with similar distribution on the passageway of these upward leader channels. For the second, it could be associated with two successive steps of one propagating channel. We note that the time interval between the two pulses of this double-peak TGF is generally consistent with the typical duration of the stepped leader’s step, i.e.,  $\sim 0.1$  ms (Lyu et al., 2016). Meanwhile, the typical length of leader steps during intracloud lightning discharge is from several hundred meters to several kilometers (Stolzenburg et al., 2016). Therefore, the second pulse of this TGF was also likely generated after the initial leader (which resulted in the first pulse) propagated forward for one or several more steps.

We also find that the overlapping pulse of a TGF could be as short as  $\sim 10 \mu\text{s}$  (Figure 4f). These fine structures in light curves provide new insights into the specific electric field distribution of lightning discharge. Since the tails of TGFs are usually soft (Nemiroff

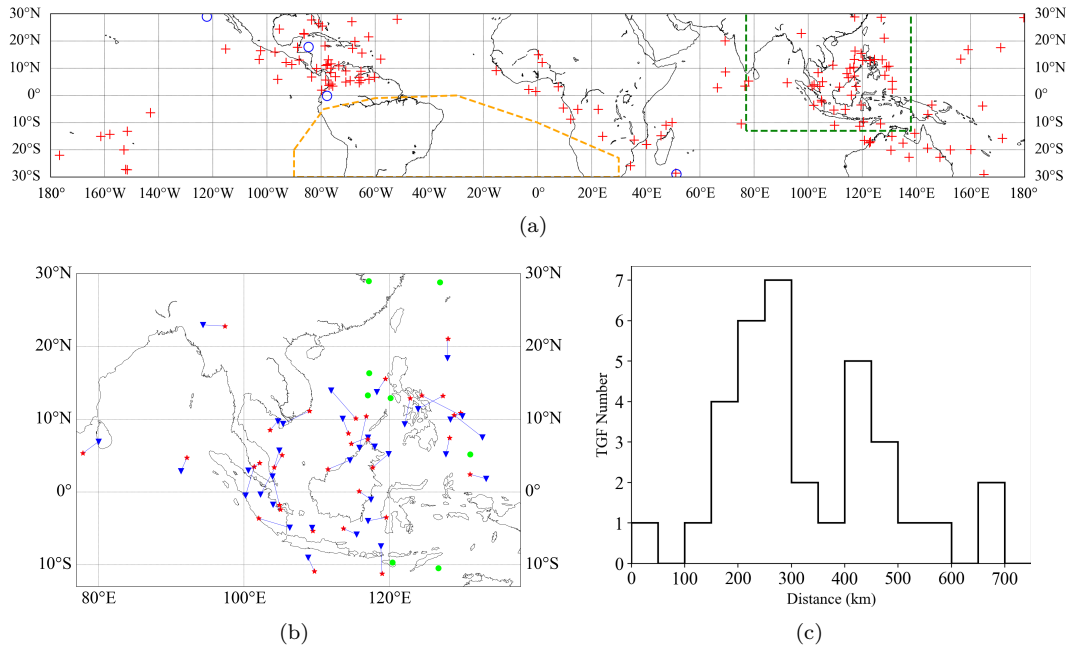


**Figure 2.** Geographical distribution of GECAM TGFs. (a) GECAM nadirs of 147 TGFs (fuchsia pluses) and 4 TEBs (blue circles). The green and orange dashed lines show the east Asia region (EAR, 77° E–138° E, 13° S–30° N) and South Atlantic Anomaly (SAA), respectively. (b) The red[ime] markers illustrate the TGFs with[without] associated GLD360 lightning inside the EAR. The blue triangles illustrate the associated lightning within  $\pm 5$  ms corrected for the light travel time and within 800 km from GECAM nadirs. (c) The distribution of sphere distance between the GECAM nadirs and their associated GLD360 lightning inside the EAR.

243  
244  
245  
246  
247  
248

et al., 1997; Feng et al., 2002), the high-gain channels of GRDs (down to  $\sim 15$  keV) are suitable to detect these tails (see Figure 4d to 4f). Furthermore, thanks to the high time resolution and a large number of GRD detectors provided by GECAM, some short-duration (down to  $37 \mu\text{s}$ ) TGFs are found, as shown in Figure 4g to 4h. There are more than 40 counts registered in such a short duration of  $37 \mu\text{s}$ , indicating an extremely high counts rate of  $\sim 1.1$  million counts/s (see Figure 4g).

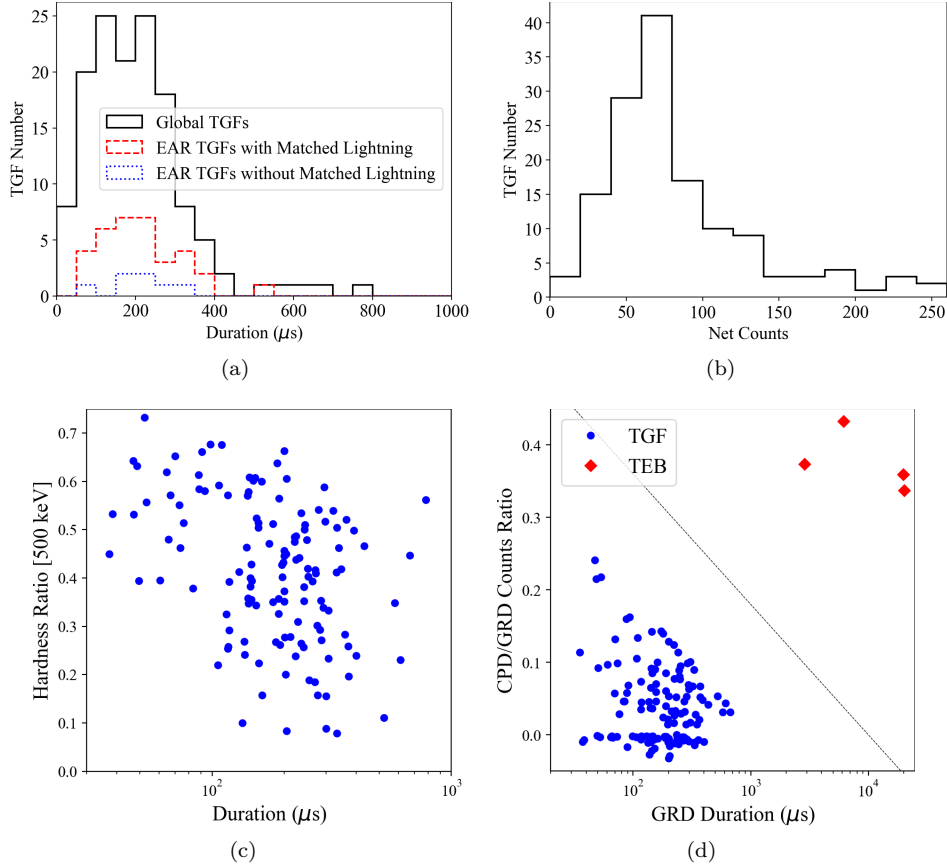


**Figure 3.** Statistical properties of GECAM TGFs and TEBs. (a) The duration distribution of TGFs. The duration is calculated by the Bayesian Blocks algorithm. The black, red, and blue lines illustrate the duration distribution of total TGFs (147), TGFs with (34), and without (8) associated GLD360 lightning in the EAR, respectively. (b) The distribution of the observed net counts for total TGFs. (c) The scatter plot of the duration of TGF events versus hardness ratio (energy limitation 500 keV). (d) The scatter plot of duration versus CPD/GRD counts ratio for TGFs and TEBs. The dashed line shows a tentative threshold of equation  $y = -0.18 \times \log_{10}(x) + 0.72$  for TGF/TEB classification, where  $x$  is the duration ( $\mu\text{s}$ ) and  $y$  is the CPD/GRD counts ratio.

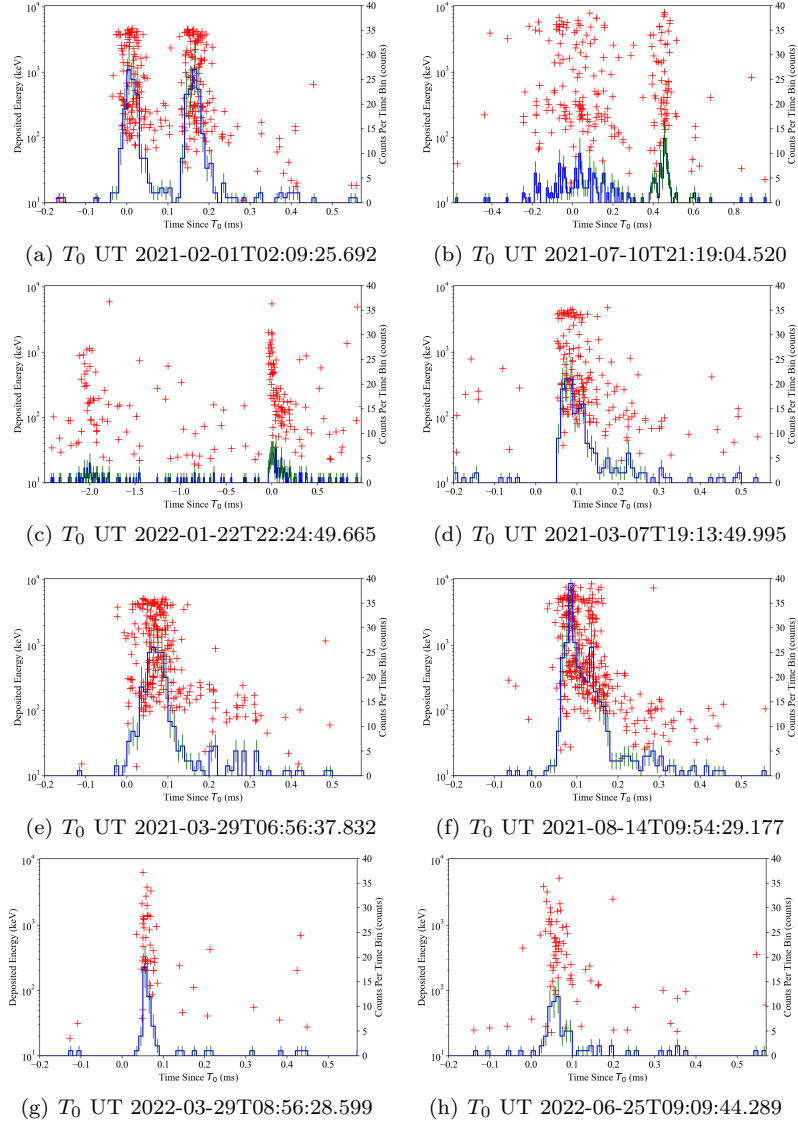


**Figure 4.** The light curves and time-energy scatters of characteristic GECAM TGFs. (a) to (c): multipeaked TGFs. (d) to (f): bright TGFs with  $> 150$  counts in duration. Note the overlapping pulse of (f). (g) to (h): short-duration TGFs ( $37 \mu\text{s}$  and  $65 \mu\text{s}$ ). The black histograms and red crosses show the light curves and time-energy scatters, respectively. The vertical and horizontal for all TGFs are on the same scales except for (b) and (c).

249 **4 GECAM TEBs**

250 The GECAM CPDs are mostly used to detect electrons and positrons in orbit, while  
 251 it has low detection efficiency to gamma-ray (Xu et al., 2022). To distinguish between  
 252 TGFs and TEBs, we find a very effective threshold considering the duration and CPD/GRD  
 253 counts ratio (see Figure 3d).

254 In this paper, we present four high-confidence TEBs, as shown in Figure 2, Fig-  
 255 ure 3d, and Figure 5. Although TEBs can also produce many counts in GRDs, their du-  
 256 ration and the CPD/GRD counts ratio is remarkably different from TGFs. It is explic-  
 257 itly shown in Figure 3d that the TEBs and TGFs are separated into two groups accord-  
 258 ing to duration and CPD/GRD counts ratio. The CPD/GRD counts ratio for all TGFs  
 259 is  $< 0.25$  and mostly  $< 0.15$ , while that of TEBs reaches  $\sim 0.35$ . It should be noticed  
 260 that the negative values of the CPD/GRD counts ratio mean no significant signals reg-  
 261 istered in CPDs. The duration of TGFs ( $< 1$  ms) and TEBs ( $> 2$  ms) are also distinc-  
 262 tively different.

263 GECAM-B detected an interesting TEB event with two pulses separated by  $\sim 150$   
 264 ms (Figure 5a) that occurred over the Southwest Indian Ocean at 18:34:40.552 UTC on  
 265 September 11th, 2021. Unlike the bright main peak and weak return peak in a typical  
 266 TEB, these two pulses have similar brightness. Since TEB electrons will travel along the  
 267 Earth's magnetic field lines, we trace this line using the International Geomagnetic Ref-  
 268 erence Field (IGRF) 13 model (Alken et al., 2021). As shown in Figure 5e and 5f, there  
 269 is no lightning activity around the GECAM nadir ( $51.2^\circ$  E,  $28.9^\circ$  S, 587.7 km) and the  
 270 southern magnetic footpoint ( $-31.3^\circ$  E,  $52.8^\circ$  N, 40 km) within  $\pm 1$  minute of the TEB  
 271 time and a radius of 1200 km. However, there is a cluster of WWLLN lightning around  
 272 the northern magnetic footpoint ( $44.1^\circ$  E,  $45.5^\circ$  N, 40 km) within 400 km and  $\pm 10$  sec-  
 273 onds. Moreover, the expected round-trip bounce time between the GECAM-B satellite  
 274 and the southern footpoint is  $< \sim 17$  ms for 100 keV electrons, which is an order of mag-  
 275 nitude lower than the observed time interval between the two pulses, strongly disfavor-  
 276 ing the return peak nature of the second pulse.

277 Considering the lack of lightning discharge in the southern part and intense light-  
 278 ning activity in the northern part, as well as the expected time interval for TEB elec-  
 279 trons, bounce from GECAM and the southern footpoint is far less than 150 ms, it is highly  
 280 likely that the TEB electrons of both pulses originate from TGFs occurred around the  
 281 northern footpoint in the same lightning discharge process. Even if they are produced  
 282 by two TGF events, the distance between these two TGFs should not be very far, oth-  
 283 erwise, they would not be detected as TEB at the same location of GECAM-B. As far  
 284 as we are aware of, this TEB is the first reported event with two pulses that originate  
 285 from the same geomagnetic footpoint.

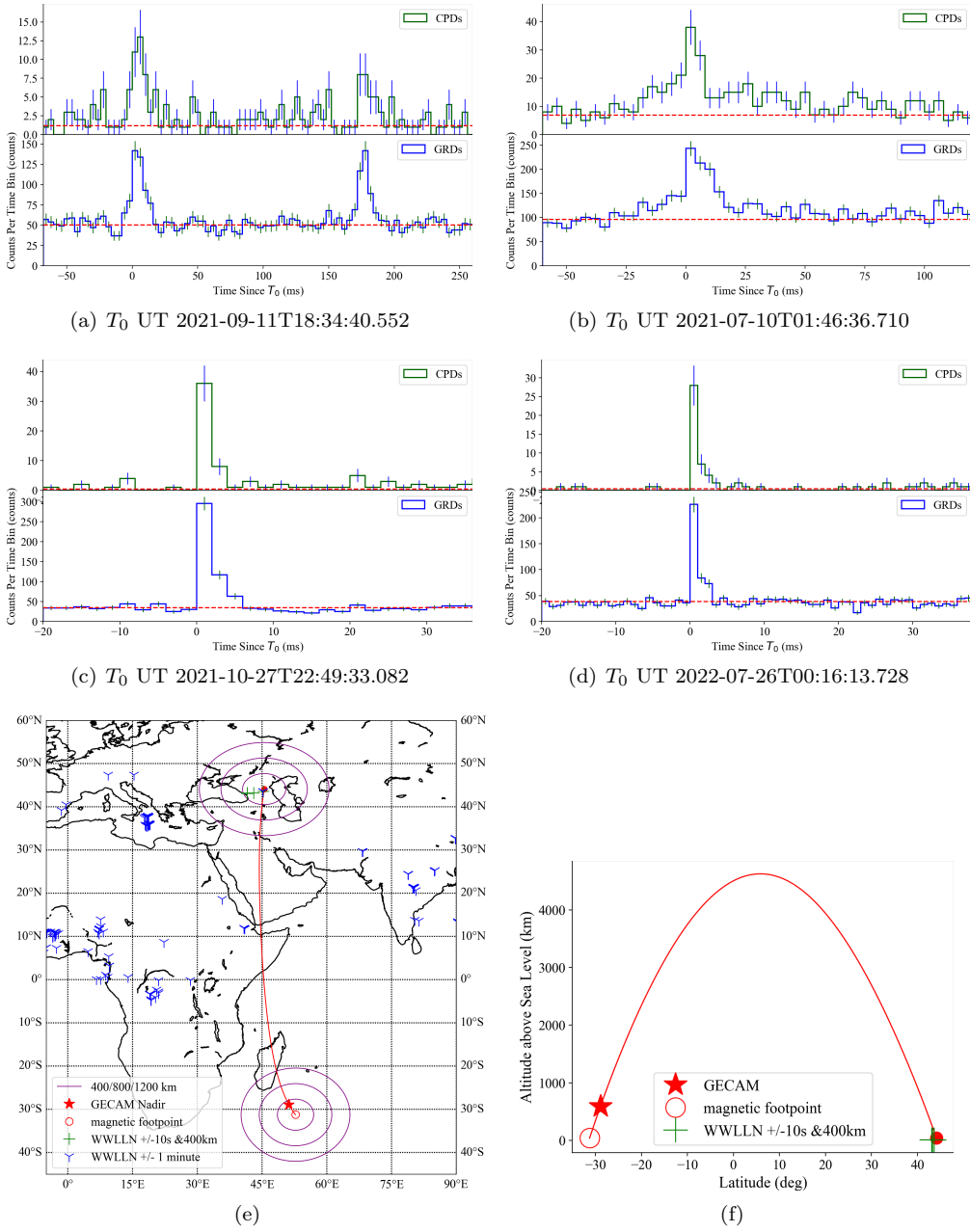


**Figure 5.** (a) to (d) The light curves of 4 GECAM TEBs. For each TEB, the upper and lower panels show the light curves of CPDs and GRDs, respectively. It should be noted that there are two pulses which episode by  $\sim 150$  ms on subfigure (a). (e) Map of GECAM nadir (red star), WWLLN lightning (blue triangles and green pluses), the traced magnetic field line (red line), and their footpoints (red circles) for the TEBs shown in subfigure (a). (f) The latitude-altitude projected map of the TEBs shown in subfigure (a). The blue triangles illustrate total WWLLN detections within 60 seconds, and green pluses illustrate the WWLLN lightning around the northern magnetic footpoint 400 km within 10 seconds. The solid red circle shows the northern magnetic footpoint and the hollow red circle shows the southern magnetic footpoint.

## 5 Conclusion

With novel designs on detectors and electronics, GECAM is a new powerful instrument to detect and identify TGFs and TEBs, as well as study their properties. Thanks to the high time resolution (100 ns), broad detection energy range (several keV to several MeV), and anti-saturation designs, GECAM can record very bright TGFs and TEBs, and reveal their fine structures in light curves and spectrum, which can help us better understand the production mechanism of TGFs and TEBs.

In this paper, a GECAM TGF/TEB search algorithm is proposed, then 147 bright TGFs and 4 TEBs are identified. The TGF detection rate for GECAM-B is  $\sim 200$  TGFs/year, which will increase if we loose the search threshold. The GECAM-GLD360 lightning-association ratio reaches  $\sim 80\%$  in the east Asia region, significantly higher than previous results obtained with the other space-borne instruments and the WWLLN data. A few interesting structures of TGFs are notable, such as a short spike (down to  $\sim 10 \mu\text{s}$ ) lying on the decay phase of the main pulse, an interesting double-peak TGF with very similar temporal and spectral distribution, and more than 40 counts are registered in an extremely short duration of  $\sim 37 \mu\text{s}$ .

For mostly gamma-ray space telescopes, determining a TEB is not straightforward, e.g. through the 511 keV line of the spectrum and the return peak. With the joint observation of GRDs and CPDs, GECAM can directly distinguish between TGFs and TEBs according to the duration distribution and CPD/GRD counts ratio. We find an interesting TEB with two pulses which probably originated from a special lightning discharge process.

## Acknowledgments

The GECAM (HuaiRou-1) mission is supported by the Strategic Priority Research Program on Space Science of the Chinese Academy of Sciences, China. This work is supported by the National Key R&D Program of China (2021YFA0718500). We thank the support from the Strategic Priority Research Program on Space Science, the Chinese Academy of Sciences (Grant No. XDA15360102, XDA15360300, XDA15052700), the National Natural Science Foundation of China (Grant No. 12273042, 12173038, 42274205, U1938115, U2038106), the National HEP Data Center (Grant No. E029S2S1) and the open fund of Hubei Luojia Laboratory (Grant No. 220100051). We thank Xi Long (Harvard University) for the helpful discussions. The GLD360 data used in this paper belong to Vaisala Inc who supports the ASIM project. The authors wish to thank the World Wide Lightning Location Network (<http://wwlln.net>) as a collaboration of more than 50 universities.

## References

- Alken, P., Thébault, E., Beggan, C. D., Amit, H., Aubert, J., Baerenzung, J., ... others (2021). International geomagnetic reference field: the thirteenth generation. *Earth, Planets and Space*, *73*(1), 1–25.
- An, Z. H., Sun, X. L., Zhang, D. L., Yang, S., Li, X. Q., Wen, X. Y., ... Zhou, X. (2022). The design and performance of grd onboard the geom satellite [Journal Article]. *Radiation Detection Technology and Methods*, *6*(1), 43–52. Retrieved from <https://doi.org/10.1007/s41605-021-00289-y> doi: 10.1007/s41605-021-00289-y
- Briggs, M. S., Fishman, G., Connaughton, V., Bhat, P., Paciesas, W., Preece, R., ... others (2010). First results on terrestrial gamma ray flashes from the fermi gamma-ray burst monitor. *Journal of Geophysical Research: Space Physics*, *115*(A7).
- Briggs, M. S., Xiong, S., Connaughton, V., Tierney, D., Fitzpatrick, G., Foley, S., ... others (2013). Terrestrial gamma-ray flashes in the fermi era: Improved observations and analysis methods. *Journal of Geophysical Research: Space Physics*, *118*(6), 3805–3830.
- Cai, C., Xiong, S. L., Li, C. K., Liu, C. Z., Zhang, S. N., Li, X. B., ... Zhou, D. K. (2021, 09). Search for gamma-ray bursts and gravitational wave electromagnetic counterparts with High Energy X-ray Telescope of Insight-HXMT. *Monthly Notices of the Royal Astronomical Society*, *508*(3), 3910–3920. Retrieved from <https://doi.org/10.1093/mnras/stab2760> doi: 10.1093/mnras/stab2760
- Cai, C., Xiong, S.-L., Xue, W.-C., Zhao, Y., Xiao, S., Yi, Q.-B., ... Zhang, F. (2022, 10). Burst search method based on likelihood ratio in Poisson statistics. *Monthly Notices of the Royal Astronomical Society*, *518*(2), 2005–2014. Retrieved from <https://doi.org/10.1093/mnras/stac3075> doi: 10.1093/mnras/stac3075
- Celestin, S., & Pasko, V. P. (2011). Energy and fluxes of thermal runaway electrons produced by exponential growth of streamers during the stepping of lightning leaders and in transient luminous events. *Journal of Geophysical Research: Space Physics*, *116*(A3).
- Celestin, S., Xu, W., & Pasko, V. (2013). Spectra of x-ray and gamma-ray bursts produced by stepping lightning leaders. In *Egu general assembly conference abstracts* (p. 13065).
- Chanrion, O., & Neubert, T. (2010). Production of runaway electrons by negative streamer discharges. *Journal of Geophysical Research: Space Physics*, *115*(A6).
- Dwyer, J. (2003). A fundamental limit on electric fields in air. *Geophysical Research Letters*, *30*(20).
- Dwyer, J. (2008). Source mechanisms of terrestrial gamma-ray flashes. *Journal of Geophysical Research: Atmospheres*, *113*(D10).
- Dwyer, J. (2012). The relativistic feedback discharge model of terrestrial gamma ray flashes. *Journal of Geophysical Research: Space Physics*, *117*(A2).
- Dwyer, J. R. (2010). Diffusion of relativistic runaway electrons and implications for lightning initiation. *Journal of Geophysical Research: Space Physics*, *115*(A3).
- Dwyer, J. R., Grefenstette, B. W., & Smith, D. M. (2008). High-energy electron beams launched into space by thunderstorms. *Geophysical Research Letters*, *35*(2).
- Dwyer, J. R., Schaal, M. M., Cramer, E., Arabshahi, S., Liu, N., Rassoul, H., ... Uman, M. A. (2012). Observation of a gamma-ray flash at ground level in association with a cloud-to-ground lightning return stroke. *Journal of Geophysical Research: Space Physics*, *117*(A10).
- Dwyer, J. R., & Smith, D. M. (2005). A comparison between monte carlo simulations of runaway breakdown and terrestrial gamma-ray flash observations.

- 376 *Geophysical Research Letters*, 32(22).
- 377 Feng, H., Li, T., Wu, M., Zha, M., & Zhu, Q. (2002). Temporal and spectral proper-  
378 ties of gamma-ray flashes. *Geophysical research letters*, 29(3), 6–1.
- 379 Fishman, G. J., Bhat, P. N., Mallozzi, R., Horack, J. M., Koshut, T., Kouveliotou,  
380 C., ... Christian, H. J. (1994). Discovery of intense gamma-ray flashes of at-  
381 mospheric origin. *Science*, 264(5163), 1313–1316. Retrieved 2022-05-05, from  
382 <http://www.jstor.org/stable/2884079>
- 383 Goldstein, A., Veres, P., Burns, E., Briggs, M. S., Hamburg, R., Kocevski, D., ...  
384 Stanbro, M. (2017, oct). An ordinary short gamma-ray burst with extraor-  
385 dinary implications: Fermi-gbm detection of grb 170817a. *The Astrophysical*  
386 *Journal*, 848(2), L14. Retrieved from [https://doi.org/10.3847/2041-8213/](https://doi.org/10.3847/2041-8213/aa8f41)  
387 [aa8f41](https://doi.org/10.3847/2041-8213/aa8f41) doi: 10.3847/2041-8213/aa8f41
- 388 Grefenstette, B. W., Smith, D. M., Hazelton, B., & Lopez, L. (2009). First rhesi  
389 terrestrial gamma ray flash catalog. *Journal of Geophysical Research: Space*  
390 *Physics*, 114(A2).
- 391 Gurevich, A., Milikh, G., & Roussel-Dupre, R. (1992). Runaway electron mechanism  
392 of air breakdown and preconditioning during a thunderstorm. *Physics Letters*  
393 *A*, 165(5-6), 463–468.
- 394 Han, X., Zhang, K., Huang, J., YU, J., XIONG, S., CHEN, Y., ... GENG, H. (2020).  
395 Gecam satellite system design and technological characteristic [Journal Ar-  
396 ticle]. *SCIENTIA SINICA Physica, Mechanica & Astronomica*, 50(1674-  
397 7275), 129507. Retrieved from [https://www.sciengine.com/publisher/](https://www.sciengine.com/publisher/ScienceChinaPress/journal/SCIENTIASINICAPhysica,Mechanica&Astronomica/50/12/10.1360/SSPMA-2020-0120)  
398 [ScienceChinaPress/journal/SCIENTIASINICAPhysica,Mechanica\](https://www.sciengine.com/publisher/ScienceChinaPress/journal/SCIENTIASINICAPhysica,Mechanica&Astronomica/50/12/10.1360/SSPMA-2020-0120)  
399 [&Astronomica/50/12/10.1360/SSPMA-2020-0120](https://www.sciengine.com/publisher/ScienceChinaPress/journal/SCIENTIASINICAPhysica,Mechanica&Astronomica/50/12/10.1360/SSPMA-2020-0120) doi: [https://doi.org/](https://doi.org/10.1360/SSPMA-2020-0120)  
400 [10.1360/SSPMA-2020-0120](https://doi.org/10.1360/SSPMA-2020-0120)
- 401 Klebesadel, R. W., Strong, I. B., & Olson, R. A. (1973). Observations of gamma-ray  
402 bursts of cosmic origin. *The Astrophysical Journal*, 182, L85.
- 403 Li, et al. (2022). The technology for detection of gamma-ray burst with GECAM  
404 satellite. *Radiation Detection Technology and Methods*. doi: 10.1007/s41605-  
405 -021-00288-z
- 406 Lindanger, A., Marisaldi, M., Maiorana, C., Sarria, D., Albrechtsen, K., Østgaard,  
407 N., ... others (2020). The 3rd agile terrestrial gamma ray flash catalog. part i:  
408 Association to lightning sferics. *Journal of Geophysical Research: Atmospheres*,  
409 125(11), e2019JD031985.
- 410 Liu, N., & Dwyer, J. R. (2013). Modeling terrestrial gamma ray flashes produced  
411 by relativistic feedback discharges. *Journal of Geophysical Research: Space*  
412 *Physics*, 118(5), 2359–2376.
- 413 Liu, Y., Gong, K., Li, X., Wen, X., An, Z., Cai, C., ... others (2021). The sipm  
414 array data acquisition algorithm applied to the gecam satellite payload. *arXiv*  
415 *preprint arXiv:2112.04786*.
- 416 Lorimer, D. R., Bailes, M., McLaughlin, M. A., Narkevic, D. J., & Crawford, F.  
417 (2007). A bright millisecond radio burst of extragalactic origin. *Science*,  
418 318(5851), 777–780.
- 419 Lu, G., Blakeslee, R. J., Li, J., Smith, D. M., Shao, X.-M., McCaul, E. W., ... Cum-  
420 mer, S. A. (2010). Lightning mapping observation of a terrestrial gamma-ray  
421 flash. *Geophysical Research Letters*, 37(11).
- 422 Lu, G., Cummer, S. A., Li, J., Han, F., Smith, D. M., & Grefenstette, B. W. (2011).  
423 Characteristics of broadband lightning emissions associated with terrestrial  
424 gamma ray flashes. *Journal of Geophysical Research: Space Physics*, 116(A3).
- 425 Lyu, F., Cummer, S. A., Lu, G., Zhou, X., & Weinert, J. (2016). Imaging lightning  
426 intracloud initial stepped leaders by low-frequency interferometric lightning  
427 mapping array. *Geophysical Research Letters*, 43(10), 5516–5523.
- 428 Maiorana, C., Marisaldi, M., Lindanger, A., Østgaard, N., Ursi, A., Sarria, D., ...  
429 others (2020). The 3rd agile terrestrial gamma-ray flashes catalog. part ii:  
430 Optimized selection criteria and characteristics of the new sample. *Journal of*

- 431 *Geophysical Research: Atmospheres*, 125(11), e2019JD031986.
- 432 Marisaldi, M., Fuschino, F., Labanti, C., Galli, M., Longo, F., Del Monte, E., ... others  
433 (2010). Detection of terrestrial gamma ray flashes up to 40 mev by the  
434 agile satellite. *Journal of Geophysical Research: Space Physics*, 115(A3).
- 435 Marisaldi, M., Galli, M., Labanti, C., Østgaard, N., Sarria, D., Cummer, S., ... others  
436 (2019). On the high-energy spectral component and fine time structure of  
437 terrestrial gamma ray flashes. *Journal of Geophysical Research: Atmospheres*,  
438 124(14), 7484–7497.
- 439 Mezentsev, A., Østgaard, N., Gjesteland, T., Albrechtsen, K., Lehtinen, N.,  
440 Marisaldi, M., ... Cummer, S. (2016). Radio emissions from double rhesi  
441 tgfs. *Journal of Geophysical Research: Atmospheres*, 121(13), 8006–8022.
- 442 Moss, G. D., Pasko, V. P., Liu, N., & Veronis, G. (2006). Monte carlo model for  
443 analysis of thermal runaway electrons in streamer tips in transient luminous  
444 events and streamer zones of lightning leaders. *Journal of Geophysical Re-*  
445 *search: Space Physics*, 111(A2).
- 446 Nemiroff, R. J., Bonnell, J. T., & Norris, J. P. (1997). Temporal and spectral char-  
447 acteristics of terrestrial gamma flashes. *Journal of Geophysical Research: Space*  
448 *Physics*, 102(A5), 9659–9665.
- 449 Østgaard, N., Neubert, T., Reglero, V., Ullaland, K., Yang, S., Genov, G., ... others  
450 (2019). First 10 months of tgf observations by asim. *Journal of Geophysical*  
451 *Research: Atmospheres*, 124(24), 14024–14036.
- 452 Poelman, D. R., Schulz, W., & Vergeiner, C. (2013). Performance characteristics of  
453 distinct lightning detection networks covering belgium. *Journal of Atmospheric*  
454 *and Oceanic Technology*, 30(5), 942–951.
- 455 Pohjola, H., & Mäkelä, A. (2013). The comparison of gld360 and euclid lightning lo-  
456 cation systems in europe. *Atmospheric research*, 123, 117–128.
- 457 Roberts, O. J., Fitzpatrick, G., Stanbro, M., McBreen, S., Briggs, M. S., Holzworth,  
458 R. H., ... Mailyan, B. G. (2018). The first fermi-gbm terrestrial gamma ray  
459 flash catalog. *Journal of Geophysical Research: Space Physics*, 123(5), 4381-  
460 4401. Retrieved from [https://agupubs.onlinelibrary.wiley.com/doi/abs/](https://agupubs.onlinelibrary.wiley.com/doi/abs/10.1029/2017JA024837)  
461 [10.1029/2017JA024837](https://doi.org/10.1029/2017JA024837) doi: <https://doi.org/10.1029/2017JA024837>
- 462 Said, R., Cohen, M., & Inan, U. (2013). Highly intense lightning over the oceans:  
463 Estimated peak currents from global gld360 observations. *Journal of Geophysi-*  
464 *cal Research: Atmospheres*, 118(13), 6905–6915.
- 465 Sarria, D., Østgaard, N., Kochkin, P., Lehtinen, N., Mezentsev, A., Marisaldi, M.,  
466 ... others (2021). Constraining spectral models of a terrestrial gamma-ray  
467 flash from a terrestrial electron beam observation by the atmosphere-space  
468 interactions monitor. *Geophysical Research Letters*, 48(9), e2021GL093152.
- 469 Scargle, J. D., Norris, J. P., Jackson, B., & Chiang, J. (2013, feb). Studies in  
470 astronomical time series analysis. vi. bayesian block representations. *The As-*  
471 *trophysical Journal*, 764(2), 167. Retrieved from [https://doi.org/10.1088/](https://doi.org/10.1088/0004-637x/764/2/167)  
472 [0004-637x/764/2/167](https://doi.org/10.1088/0004-637x/764/2/167) doi: 10.1088/0004-637x/764/2/167
- 473 Skeltved, A. B., Østgaard, N., Mezentsev, A., Lehtinen, N., & Carlson, B. (2017).  
474 Constraints to do realistic modeling of the electric field ahead of the tip of  
475 a lightning leader. *Journal of Geophysical Research: Atmospheres*, 122(15),  
476 8120–8134.
- 477 Stolzenburg, M., Marshall, T. C., Karunarathne, S., & Orville, R. E. (2016). Lumi-  
478 nosity with intracloud-type lightning initial breakdown pulses and terrestrial  
479 gamma-ray flash candidates. *Journal of Geophysical Research: Atmospheres*,  
480 121(18), 10–919.
- 481 Ursi, A., Guidorzi, C., Marisaldi, M., Sarria, D., & Frontera, F. (2017). Terrestrial  
482 gamma-ray flashes in the beposax data archive. *Journal of Atmospheric and*  
483 *Solar-Terrestrial Physics*, 156, 50–56.
- 484 Wilson, C. T. (1925). The acceleration of  $\beta$ -particles in strong electric fields such  
485 as those of thunderclouds. In *Mathematical proceedings of the cambridge philo-*

- 486 *sophical society* (Vol. 22, pp. 534–538).
- 487 Woods, P., & Thompson, C. (2004). Soft gamma repeaters and anomalous x-ray  
488 pulsars: magnetar candidates. *arXiv preprint astro-ph/0406133*.
- 489 Xiao, S., Liu, Y., Peng, W., An, Z., Xiong, S., Tuo, Y., ... others (2022). On-ground  
490 and on-orbit time calibrations of gecam. *Monthly Notices of the Royal Astro-*  
491 *nomical Society*, 511(1), 964–971.
- 492 Xiong, S., Briggs, M., Connaughton, V., Fishman, G., Tierney, D., Fitzpatrick,  
493 G., ... Hutchins, M. (2012). Location prediction of electron tgfs. *Journal of*  
494 *Geophysical Research: Space Physics*, 117(A2).
- 495 Xu, W., Celestin, S., & Pasko, V. P. (2012). Source altitudes of terrestrial gamma-  
496 ray flashes produced by lightning leaders. *Geophysical Research Letters*, 39(8).
- 497 Xu, W., Celestin, S., & Pasko, V. P. (2015). Optical emissions associated with  
498 terrestrial gamma ray flashes. *Journal of Geophysical Research: Space Physics*,  
499 120(2), 1355–1370.
- 500 Xu, Y. B., Li, X. Q., Sun, X. L., Yang, S., Wang, H., Peng, W. X., ... Zhou, X.  
501 (2022). The design and performance of charged particle detector onboard the  
502 gecam mission [Journal Article]. *Radiation Detection Technology and Methods*,  
503 6(1), 53-62. Retrieved from <https://doi.org/10.1007/s41605-021-00298-x>  
504 doi: 10.1007/s41605-021-00298-x
- 505 Zhang, et al. (2022). Dedicated sipm array for grd of gecam. *Radiation Detection*  
506 *Technology and Methods*, 6(1), 63–69.
- 507 Zhao, X., Xiong, S., Wen, X., Li, X., Cai, C., Xiao, S., & Luo, Q. (2021, December).  
508 The In-Flight Realtime Trigger and Localization Software of GECAM. *arXiv*  
509 *e-prints*, arXiv:2112.05101.
- 510 Zhao, Y., Xue, W., Xiong, S., Luo, Q., YQ, Z., H, Y., ... SN, Z. (2022, September).  
511 On the Localization Methods of High Energy Transients for All-Sky Gamma-  
512 Ray Monitors. *arXiv e-prints*, arXiv:2209.13088.
- 513 Zhao, Y., Xue, W., Xiong, S., Wang, Y., Liu, J., Luo, Q., ... Yu, H. (2022, Novem-  
514 ber). GECAM Localization of High Energy Transients and the Systematic Er-  
515 ror. *arXiv e-prints*, arXiv:2211.15570.

# The First GECAM Observation Results on Terrestrial Gamma-ray Flashes and Terrestrial Electron Beams

Y. Zhao<sup>1,2</sup>, J. C. Liu<sup>2,3</sup>, S. L. Xiong<sup>2</sup>, W. C. Xue<sup>2,3</sup>, Q. B. Yi<sup>4,2</sup>, G. P. Lu<sup>5</sup>, W. Xu<sup>6</sup>, F. C. Lyu<sup>7</sup>, J. C. Sun<sup>2</sup>, W. X. Peng<sup>2</sup>, C. Zheng<sup>2,3</sup>, Y. Q. Zhang<sup>2,3</sup>, C. Cai<sup>8</sup>, S. Xiao<sup>9,10</sup>, S. L. Xie<sup>11</sup>, C. W. Wang<sup>2,3</sup>, W. J. Tan<sup>2,3</sup>, Z. H. An<sup>2</sup>, G. Chen<sup>2</sup>, Y. Q. Du<sup>12,2</sup>, Y. Huang<sup>2</sup>, M. Gao<sup>2</sup>, K. Gong<sup>2</sup>, D. Y. Guo<sup>2</sup>, J. J. He<sup>2</sup>, B. Li<sup>2</sup>, G. Li<sup>2</sup>, X. Q. Li<sup>2</sup>, X. B. Li<sup>2</sup>, J. Liang<sup>12,2</sup>, X. H. Liang<sup>2</sup>, Y. Q. Liu<sup>2</sup>, X. Ma<sup>2</sup>, R. Qiao<sup>2</sup>, L. M. Song<sup>2</sup>, X. Y. Song<sup>2</sup>, X. L. Sun<sup>2</sup>, J. Wang<sup>2</sup>, J. Z. Wang<sup>2</sup>, P. Wang<sup>2</sup>, X. Y. Wen<sup>2</sup>, H. Wu<sup>12,2</sup>, Y. B. Xu<sup>2</sup>, S. Yang<sup>2</sup>, B. X. Zhang<sup>2</sup>, D. L. Zhang<sup>2</sup>, F. Zhang<sup>2</sup>, P. Zhang<sup>13,2</sup>, H. M. Zhang<sup>2</sup>, Z. Zhang<sup>2</sup>, X. Y. Zhao<sup>2</sup>, S. J. Zheng<sup>2</sup>, K. K. Zhang<sup>14</sup>, X. B. Han<sup>14</sup>, H. Y. Wu<sup>15</sup>, T. Hu<sup>15</sup>, H. Geng<sup>15</sup>, F. J. Lu<sup>2</sup>, S. N. Zhang<sup>2</sup>, H. Yu<sup>1</sup>

<sup>1</sup>Department of Astronomy, Beijing Normal University, Beijing 100875, Beijing, China

<sup>2</sup>Key Laboratory of Particle Astrophysics, Institute of High Energy Physics, Chinese Academy of Sciences, Beijing 100049, Beijing, China

<sup>3</sup>University of Chinese Academy of Sciences, Beijing 100049, Beijing, China

<sup>4</sup>School of Physics and Optoelectronics, Xiangtan University, Xiangtan 411105, Hunan, China

<sup>5</sup>School of Earth and Space Sciences, University of Science and Technology of China, Hefei 230026, Anhui, China

<sup>6</sup>Electronic Information School, Wuhan University, Wuhan 430072, Hubei, China

<sup>7</sup>Key Laboratory of Transportation Meteorology of China Meteorological Administration, Nanjing Joint Institute for Atmospheric Sciences, Nanjing 210000, Jiangsu China

<sup>8</sup>College of Physics and Hebei Key Laboratory of Photophysics Research and Application, Hebei Normal University, Shijiazhuang, Hebei 050024, China

<sup>9</sup>Guizhou Provincial Key Laboratory of Radio Astronomy and Data Processing, Guizhou Normal University, Guiyang 550001, GuiZhou, China

<sup>10</sup>School of Physics and Electronic Science, Guizhou Normal University, Guiyang 550001, GuiZhou, China

<sup>11</sup>Institute of Astrophysics, Central China Normal University, Wuhan 430079, HuBei, China

<sup>12</sup>School of Computing and Artificial Intelligence, Southwest Jiaotong University, Chengdu 611756, SiChuan, China

<sup>13</sup>College of Electronic and Information Engineering, Tongji University, Shanghai 201804, Shanghai, China

<sup>14</sup>Innovation Academy for Microsatellites of Chinese Academy of Sciences, Shanghai 201304, Shanghai, China

<sup>15</sup>National Space Science Center, Chinese Academy of Sciences, Beijing 100190, Beijing, China

## Key Points:

- GECAM can well classify and distinguish TGF/TEB, and reveal their fine temporal and spectral features, e.g. short spikes down to 10 ms.
- GECAM discovered an interesting two-peaked TEB which is probably from a lightning process near the geomagnetic footprint.
- TGF-lightning association rate between GECAM and GLD360 in east Asia is found to be  $\sim 80\%$ , notably higher than previous reports.

---

Corresponding author: S. L. Xiong, xiongs1@ihep.ac.cn

**Abstract**

Gravitational wave high-energy Electromagnetic Counterpart All-sky Monitor (GECAM) is a space-borne instrument dedicated to monitoring high-energy transients, therewith Terrestrial Gamma-ray Flashes (TGFs) and Terrestrial Electron Beams (TEBs). We propose a TGF/TEB search algorithm, with which 147 bright TGFs and 4 TEBs are identified during an effective observation time of  $\sim 9$  months. We show that, with gamma-ray and charged particle detectors, GECAM can effectively identify and distinguish TGFs and TEBs, and measure their temporal and spectral properties in detail. Moreover, we find an interesting TEB consisting of two pulses with a separation of  $\sim 150$  ms, which is expected to originate from a lightning process near the geomagnetic footprint. We also find that the GECAM TGF's lightning-association ratio is  $\sim 80\%$  in the east Asia region using the GLD360 lightning network, which is significantly higher than previous observations.

**Plain Language Summary**

Terrestrial gamma-ray flashes (TGFs) and Terrestrial Electron Beams (TEBs) are one of the most energetic radioactive phenomena in the atmosphere of the Earth. They reflect a natural particle accelerator that can boost electrons up to at least several tens of mega electron volts (MeV). With novel detection technologies, GECAM is a new powerful instrument to observe TGFs and TEBs, as well as study their properties. For example, it is difficult for most space-borne high-energy instruments to distinguish between TGFs and TEBs. With the joint observation of gamma-ray and charged particle detectors, GECAM can effectively identify TGFs and TEBs. GECAM can also reveal fine features in the light curves and spectra of these bursts. Interestingly, GECAM discovered the first, as far as we are aware of, TEB which consists of two pulses with a separation time of about 150 ms. Unlike the case in previous TEBs, the second pulse is not the return peak but has the same origin as the first one.

**1 Introduction**

Terrestrial Gamma-ray Flashes (TGFs) are submillisecond intense bursts of  $\gamma$ -rays with energies up to several tens of MeV (Briggs et al., 2010; Marisaldi et al., 2010, 2019), which was serendipitously discovered by the Burst and Transient Source Experiment (BATSE) aboard Compton Gamma-ray Observatory (CGRO) in 1991 (Fishman et al., 1994). Since then, TGFs have been routinely observed by space-borne instruments, such as BeppoSAX (Ursi et al., 2017), RHESSI (Grefenstette et al., 2009), AGILE (Marisaldi et al., 2010), *Fermi*/GBM (Roberts et al., 2018) and ASIM (Østgaard et al., 2019) during last three decades. Occasionally, TGFs can also be observed by ground instruments (Dwyer et al., 2012), however, the strong absorption of gamma-rays in the air makes the detection very difficult.

TGFs observed by these space-borne instruments are widely believed to be produced through the initial upward leader of positive Intracloud (+IC) lightning (Lu et al., 2010, 2011). They are the results of relativistic electrons that produce hard X/ $\gamma$ -rays through the bremsstrahlung process. These electrons are accelerated in a very high electric field by the runaway process (Wilson, 1925) and multiplied by many orders of magnitude through the Relativistic Runaway Electron Avalanche process (Gurevich et al., 1992; Dwyer & Smith, 2005). Two main models were proposed to explain the production of TGFs. One is the lightning leader model, which involves the acceleration of free electrons under the localized electric field in front of lightning leader tips (Moss et al., 2006; Dwyer, 2010; Celestin & Pasko, 2011; Celestin et al., 2013). The other one is the relativistic feedback model (RFD) (Dwyer, 2003; Dwyer, 2008, 2012; Liu & Dwyer, 2013), which considers the feedback processes from positrons and photons in a large-scale electric field region.

92 However, the specific mechanism to produce  $\sim 10^{17}$  to  $10^{19}$  electrons is still an open ques-  
93 tion (Chanrion & Neubert, 2010; Xu et al., 2012, 2015; Skeltved et al., 2017).

94 By interacting with the atmosphere during the propagation, the TGF photons can  
95 produce secondary electrons and positrons. Then they will move along the Earth's mag-  
96 netic field line, forming Terrestrial Electron Beams (TEBs) (Dwyer et al., 2008), which  
97 could be observed by some TGF-detecting instruments (Xiong et al., 2012; Lindanger  
98 et al., 2020; Sarria et al., 2021).

99 In this study, the data of Gravitational-wave high-energy Electromagnetic Coun-  
100 terpart All-sky Monitor (GECAM) (Li et al., 2022) are utilized for TGFs and TEBs re-  
101 search. GECAM is a space-based instrument dedicated to the observation of gamma-  
102 ray electromagnetic counterparts of the Gravitational Waves (Goldstein et al., 2017) and  
103 Fast Radio Bursts (Lorimer et al., 2007), as well as other high-energy astrophysical and  
104 terrestrial transient sources, such as Gamma-ray Bursts (GRBs) (Klebesadel et al., 1973),  
105 Soft Gamma-ray Repeaters (SGRs) (Woods & Thompson, 2004), solar flares, TGFs and  
106 TEBs.

107

## 2 Instrument and Search Algorithm

Since the launch in December 2020, GECAM has been operating in low earth orbit (600 km altitude and 29° inclination angle) (Han et al., 2020). GECAM consists of twin micro-satellites (i.e. GECAM-A and GECAM-B) and each of them comprises 25 Gamma-ray Detectors (GRDs) (An et al., 2022) and 8 Charged Particle Detectors (CPDs) (Xu et al., 2022). It should be noted that only GECAM-B data are utilized in this study because GECAM-A has not been able to observe yet (Li et al., 2022).

With LaBr<sub>3</sub> crystals read out by silicon photomultiplier (SiPM) arrays, GRDs can detect high-energy photons in a broad energy range of  $\sim 15$  keV to  $\sim 5$  MeV (Zhang et al., 2022). CPDs are designed to detect the charged particles from  $\sim 100$  keV to  $\sim 5$  MeV. The joint observation of GRDs and CPDs can distinguish between gamma-rays and charged particle bursts, such as TGFs and TEBs (Zhao et al., 2021).

To detect those extremely short and bright bursts, e.g. TGFs and TEBs, a dedicated anti-saturation data acquisition system (DAQ) is designed for GECAM. The data buffer in DAQ can accommodate up to 4092 and 1020 counts for the high-gain and low-gain of each GRD, respectively. Since there are usually several hundred counts registered for a bright TGF, the GECAM DAQ can guarantee to transfer and save almost all TGFs photons that are recorded by detectors (Liu et al., 2021).

For GRD, the dead time is 4  $\mu$ s for normal events and  $> 69$   $\mu$ s for overflow events (i.e. events with higher energy deposition than the maximum measurable energy). Each GRD detector has two read-out channels: high-gain channel ( $\sim 15$  keV to  $\sim 300$  keV) and low-gain channel ( $\sim 300$  keV to  $\sim 5$  MeV) (Liu et al., 2021). The design, performance, and other information about GECAM have been reported by Li et al. (2022); An et al. (2022); Xu et al. (2022).

The considerable number of GRD detectors is helpful to locate the source region of TGFs. We have proposed a dedicated localization method for all-sky monitor which can be used for extremely short-duration TGFs (Zhao et al. 2022a). Despite the low counting statistics of TGFs, GECAM can still locate TGFs (Zhao et al. 2022b).

As the main contamination source for TGFs, cosmic-ray events show very similar patterns in data as TGFs, but with an even shorter duration. Thanks to the high time resolution of GECAM, i.e. 100 ns (Xiao et al., 2022), GECAM can effectively distinguish between cosmic-ray events and TGFs. Indeed, a dedicated data product called Simultaneous Events is designed for GECAM. The Simultaneous Events Number (SimEvtNum) is defined as the number of events from different detectors registered in the same 300 ns time window (Xiao et al., 2022). As the SimEvtNum increases, the probability of these events caused by cosmic-rays surges. Here a relatively loose criterion (SimEvtNum  $> 13$ ) is adopted for basic data selection.

To unveil TGFs and TEBs in GECAM data, we developed a dedicated burst search algorithm, which is very different from normal burst search for gamma-ray bursts (Cai et al., 2021, 2022), because the TGF and TEB are so weak that only a few counts are registered in each detector, and both GRDs and CPDs are needed in the search. The event-by-event (EVT) data of GECAM GRDs and CPDs are used in this study. Only recommended normal events with SimEvtNum  $< 13$  are utilized. We divide 25 GRDs into four groups considering the neighboring position, and it turns out that there are 6 [7] GRDs for 3 [1] group(s). All 8 CPDs are treated as a single group.

Assuming the background follows the Poisson distribution, the probability that the counts are from background fluctuation can be calculated as,

$$P_{\text{group}}(S \geq S' | B) = 1 - \sum_{S=0}^{S=S'-1} \frac{B^S \cdot \exp(-B)}{S!}, \quad (1)$$

155 where  $S$  and  $S'$  are observed counts and threshold counts, respectively, for one group  
 156 in a time window,  $B$  is the estimated background for the time window calculated by the  
 157 average counts over  $T_{\text{rela}} \in [-5, -1]$  s and  $\in [+1, +5]$  s, where  $T_{\text{rela}}$  is the relative time with  
 158 respect to the end time of the time window.

159 For an individual searching bin, the joint probability of at least  $N'_{\text{trig}}$  group(s) out  
 160 of total group number  $M$  passing the trigger threshold for a single group  $P_{\text{group}}$  is,

$$P_{\text{bin}}(N_{\text{trig}} \geq N'_{\text{trig}}) = \sum_{N_{\text{trig}}=N'_{\text{trig}}}^{N_{\text{trig}}=M} C_M^{N_{\text{trig}}} \cdot (P_{\text{group}})^{N_{\text{trig}}} \cdot (1 - P_{\text{group}})^{M - N_{\text{trig}}}. \quad (2)$$

161 In this work, seven time scales are utilized to do searching. The widths of time scales  
 162 with the corresponding empirical threshold  $P_{\text{tot}}$  are: 50  $\mu\text{s}$  ( $5.0 \times 10^{-22}$ ), 100  $\mu\text{s}$  ( $2.0 \times$   
 163  $10^{-21}$ ), 250  $\mu\text{s}$  ( $1.3 \times 10^{-20}$ ), 500  $\mu\text{s}$  ( $5.0 \times 10^{-20}$ ), 1 ms ( $2.0 \times 10^{-19}$ ), 2 ms ( $8.0 \times 10^{-19}$ ),  
 164 4 ms ( $3.2 \times 10^{-18}$ ). All of them are used for TGF search while only the latter four are  
 165 for TEB search. It should be noted that these empirical criteria are relatively strict so  
 166 that only intense TGFs or TEBs could be identified.

167 By setting  $P_{\text{tot}} = P_{\text{bin}}$ , the group's trigger threshold ( $P_{\text{group,GRD}}$ ) can be obtained  
 168 for TGF with GRDs from the following equation (i.e.  $M = 4$ , and we set  $N'_{\text{trig,GRD}} =$   
 169 2),

$$P_{\text{tot,GRD}}(N_{\text{trig}} \geq 2) = 6 \cdot P_{\text{group,GRD}}^2 - 8 \cdot P_{\text{group,GRD}}^3 + 3 \cdot P_{\text{group,GRD}}^4, \quad (3)$$

170 and the trigger threshold from the following equation of TEB with CPDs ( $M = 1$ , and  
 171 we set  $N'_{\text{trig,CPD}} = 1$ ),

$$P_{\text{tot,CPD}} = P_{\text{group,CPD}}. \quad (4)$$

172 According to the empirical threshold above, the trigger threshold for each detector group  
 173 can be obtained for each searching window, e.g. for 100  $\mu\text{s}$ ,  $P_{\text{group,GRD}} = 1.8 \times 10^{-11}$   
 174 which corresponds to 6.6  $\sigma$  in standard Gaussian distribution.

175 For a candidate to be identified as a TGF/TEB, all criteria below must be met:

- 176 1. The trigger threshold (Equations 3 and 4) must be satisfied.
- 177 2. The candidate should not be SGR. It should be noticed that millisecond-duration  
 178 SGRs can be searched in the time scale of milliseconds with a much softer spec-  
 179 trum than TGFs.
- 180 3. Should not be caused by instrument effects, which are characterized by that there  
 181 is significant excess (Poisson significance  $> 6 \sigma$ ) registered in 2 to 3 GRDs while  
 182 no obvious signals (Poisson significance  $< 3 \sigma$ ) for most (i.e.  $> 21$ ) GRDs.
- 183 4. For filtering out cosmic-rays, the ratio of the simultaneous event ( $R_{\text{sim},7}^1$ ) should  
 184 be  $< 20\%$ .

---

<sup>1</sup>  $R_{\text{sim},7}$ : the total number of simultaneous events registered in  $> 7$  GRDs, divided by the total events number in the searching bin.

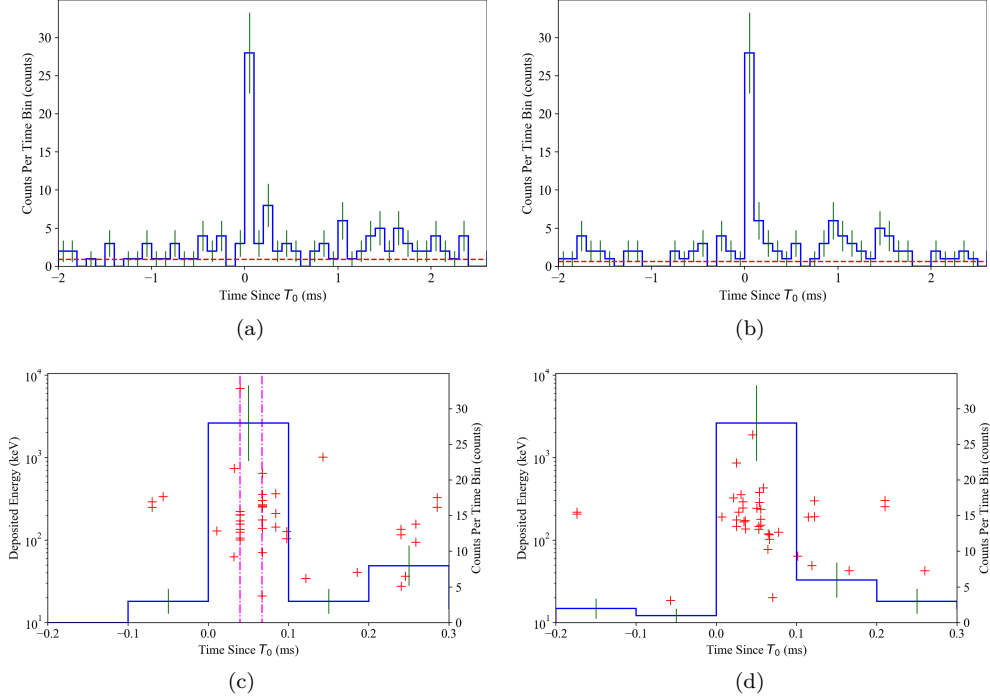


**Figure 1.** Illustration of distinguishing between cosmic-rays and TGFs by simultaneous events. (a) and (c): the light curve and time-energy scatter plot of a cosmic-ray event. (b) and (d): the light curve and time-energy scatter plot of a TGF. The dot-dashed lines show the time edge of simultaneous events registered in  $> 7$  GRDs within 300 ns. The horizontal and vertical scales are the same for the two events.

185  
186  
187  
188  
189  
190

For the identification of TEBs, more criteria are needed which will be described in Section 4. To further illustrate the capability of GECAM to identify cosmic-rays, a case is illustrated in Figure 1. The classification of the two excesses can not be distinguished well just according to the light curves. However, the cosmic-ray event (Figure 1a and 1c) has  $F_{\text{sim},7} = \frac{18}{28} \approx 64\%$ , while TGFs have no simultaneous events registered in  $> 7$  GRDs (Figure 1b and 1d).

### 3 GECAM TGFs

From December 10th, 2020 to August 31st, 2022, the effective observation time of GECAM-B is  $\sim 274.5$  days ( $\sim 0.75$  years). As shown in Figure 2, 147 bright TGFs are identified by our search algorithm, corresponding to a discovery rate of  $\sim 200$  TGFs/year or 0.54 TGFs/day. The Global Lightning Dataset (GLD360) is utilized to match lightning for GECAM TGFs in the time window of  $\pm 5$  ms corrected for the light propagation time and within the distance window of 800 km from GECAM nadirs. The GLD360 lightning-association ratio is  $\frac{34}{42} \approx 80\%$  in the east Asia region (EAR,  $77^\circ$  E– $138^\circ$  E,  $13^\circ$  S– $30^\circ$  N) which is  $\sim 2.5$  times of the results based on the data of the other spaceborne instruments and the World Wide Lightning Location Network (WWLLN) lightning ( $\sim 33\%$ ) (Roberts et al., 2018; Maiorana et al., 2020). The high lightning-association ratio may be attributed to two factors: (1) the detection efficiency of GLD360 is higher than the other lightning location network at least in EAR (Said et al., 2013; Poelman et al., 2013; Pohjola & Mäkelä, 2013), (2) the current GECAM TGF sample only contains bright ones, resulting from the very strict searching threshold. The sphere distance between the GECAM nadirs and the associated GLD360 lightning inside the EAR ranges from  $\sim 50$  km to 800 km, which is consistent with previous reports.

The statistical distribution of temporal, intensity and energy properties of this GECAM TGF sample are shown in Figure 3. The duration is calculated by the Bayesian Block (BB) algorithm (Scargle et al., 2013). Since the relatively strict threshold, faint TGFs are dropped from the current sample. Therefore, the GECAM TGF discovery rate would increase as we decrease the search threshold in the future. As shown in Figure 3c, TGF events with relatively shorter duration tend to have a harder spectrum and thus more high-energy electrons in the source region, which is in line with previous observations (Briggs et al., 2013). As shown in Figure 3d, the duration and CPD/GRD counts ratio is very effective to classify TGFs and TEBs (see Section 4).

In Figure 4, the light curves and time-energy scatter plots are illustrated for three multipeak, three bright, and two short TGFs. The fraction of multipeak TGFs is  $\frac{3}{147} \approx 2\%$ , which is consistent with that observed by the other instruments (Mezentsev et al., 2016; Lindanger et al., 2020). Since the upward leader channel of a lightning discharge would generally branch into several channels during propagation, it is widely accepted that the temporal structures may reflect the electric field distribution that the leaders have passed through. This effect is more pronounced in the multipeak or overlapping structures of TGFs.

It is worth noticing an interesting double-peaked TGF (Figure 4a) which is characterized by two  $\sim 100 \mu\text{s}$  pulses with very similar temporal and spectral structures. Two possible scenarios may explain this double-peaked TGF. For the first, it could be associated with two leader branches propagating in two distinct localized electric fields, which could be also responsible for the cases shown in Figure 4b to 4c. However, this double-peak TGF (Figure 4a) may require coincidences comparing to other TGFs in Figure 4b to 4c, i.e. two intracloud electric fields with similar distribution on the passageway of these upward leader channels. For the second, it could be associated with two successive steps of one propagating channel. We note that the time interval between the two pulses of this double-peak TGF is generally consistent with the typical duration of the stepped leader's step, i.e.,  $\sim 0.1$  ms (Lyu et al., 2016). Meanwhile, the typical length of leader steps during intracloud lightning discharge is from several hundred meters to several kilometers (Stolzenburg et al., 2016). Therefore, the second pulse of this TGF was also likely generated after the initial leader (which resulted in the first pulse) propagated forward for one or several more steps.

We also find that the overlapping pulse of a TGF could be as short as  $\sim 10 \mu\text{s}$  (Figure 4f). These fine structures in light curves provide new insights into the specific electric field distribution of lightning discharge. Since the tails of TGFs are usually soft (Nemiroff

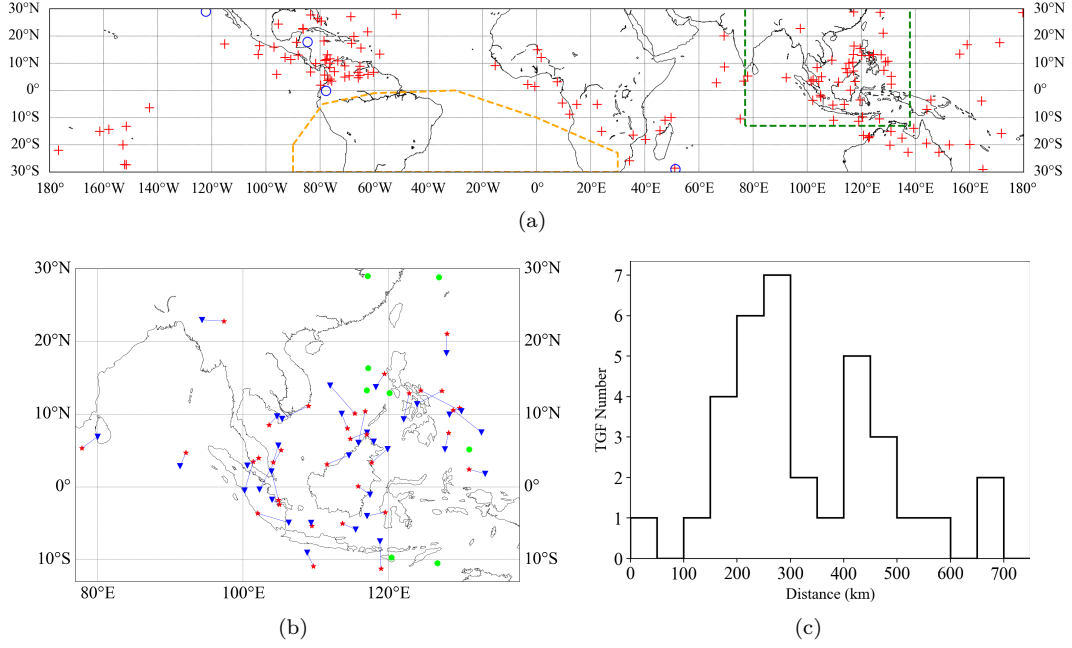


**Figure 2.** Geographical distribution of GECAM TGFs. (a) GECAM nadirs of 147 TGFs (fuchsia pluses) and 4 TEBs (blue circles). The green and orange dashed lines show the east Asia region (EAR, 77° E–138° E, 13° S–30° N) and South Atlantic Anomaly (SAA), respectively. (b) The red markers illustrate the TGFs with associated GLD360 lightning inside the EAR. The blue triangles illustrate the associated lightning within  $\pm 5$  ms corrected for the light travel time and within 800 km from GECAM nadirs. (c) The distribution of sphere distance between the GECAM nadirs and their associated GLD360 lightning inside the EAR.

243 et al., 1997; Feng et al., 2002), the high-gain channels of GRDs (down to  $\sim 15$  keV) are  
 244 suitable to detect these tails (see Figure 4d to 4f). Furthermore, thanks to the high time  
 245 resolution and a large number of GRD detectors provided by GECAM, some short-duration  
 246 (down to  $37 \mu\text{s}$ ) TGFs are found, as shown in Figure 4g to 4h. There are more than 40  
 247 counts registered in such a short duration of  $37 \mu\text{s}$ , indicating an extremely high counts  
 248 rate of  $\sim 1.1$  million counts/s (see Figure 4g).

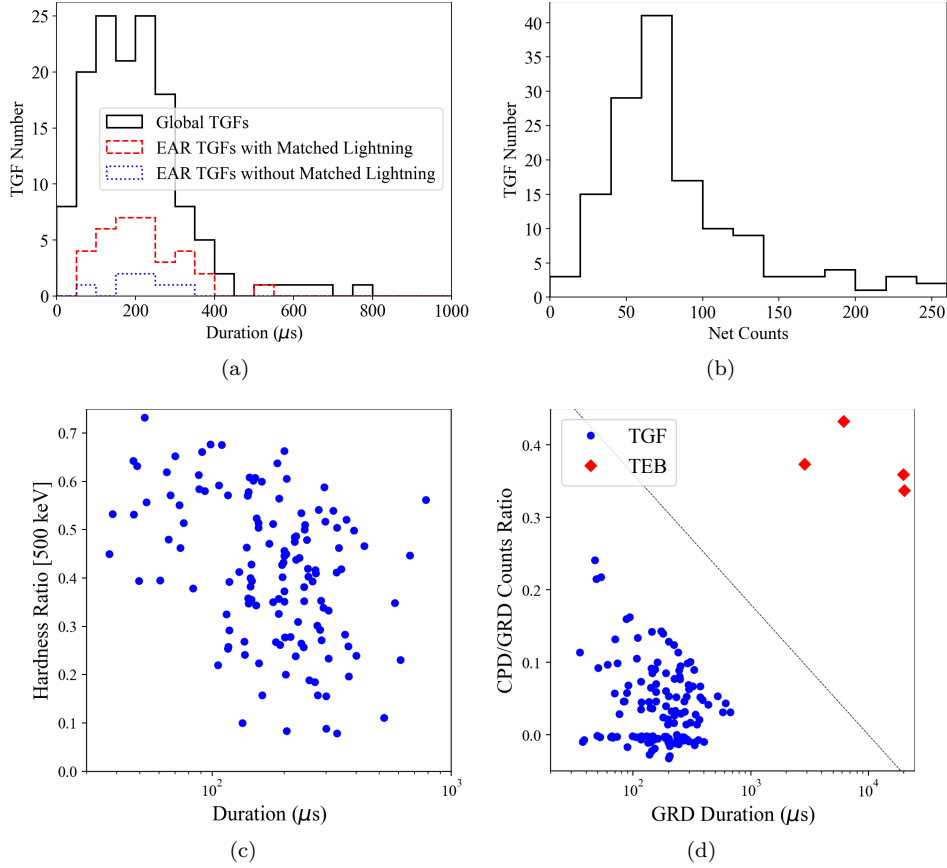


**Figure 3.** Statistical properties of GECAM TGFs and TEBs. (a) The duration distribution of TGFs. The duration is calculated by the Bayesian Blocks algorithm. The black, red, and blue lines illustrate the duration distribution of total TGFs (147), TGFs with (34), and without (8) associated GLD360 lightning in the EAR, respectively. (b) The distribution of the observed net counts for total TGFs. (c) The scatter plot of the duration of TGF events versus hardness ratio (energy limitation 500 keV). (d) The scatter plot of duration versus CPD/GRD counts ratio for TGFs and TEBs. The dashed line shows a tentative threshold of equation  $y = -0.18 \times \log_{10}(x) + 0.72$  for TGF/TEB classification, where  $x$  is the duration ( $\mu\text{s}$ ) and  $y$  is the CPD/GRD counts ratio.

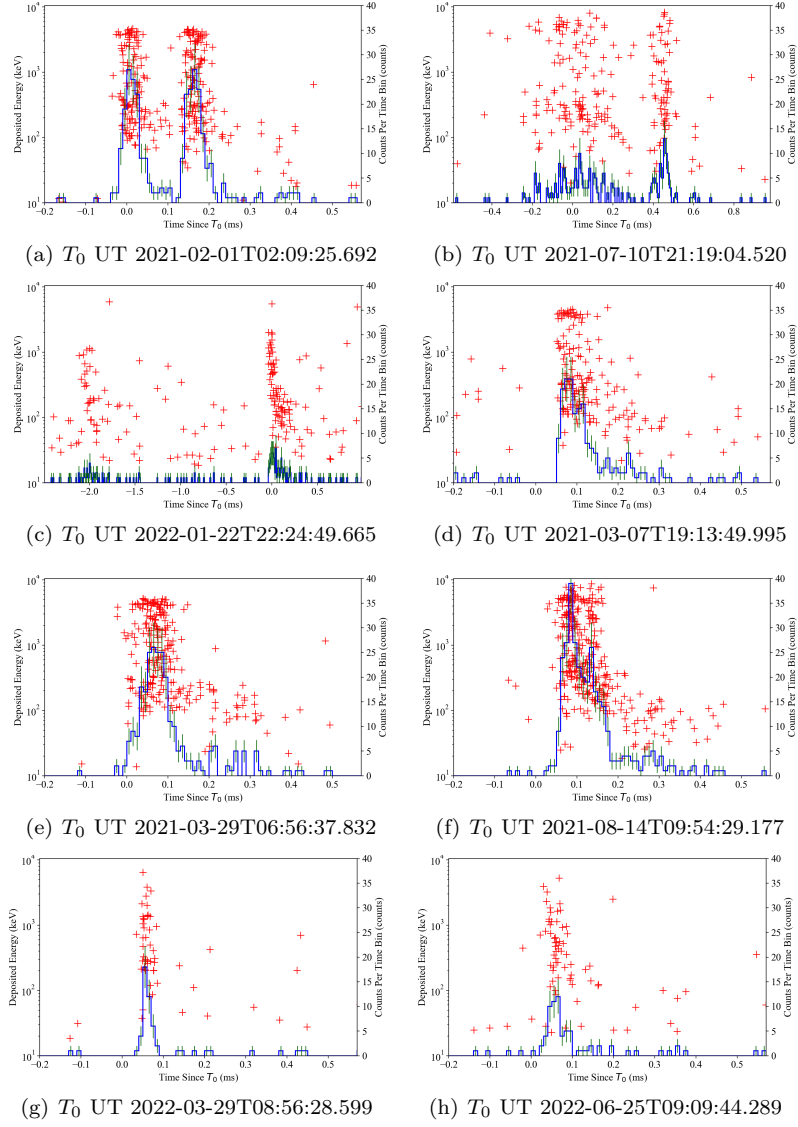


**Figure 4.** The light curves and time-energy scatters of characteristic GECAM TGFs. (a) to (c): multipeak TGFs. (d) to (f): bright TGFs with  $> 150$  counts in duration. Note the overlapping pulse of (f). (g) to (h): short-duration TGFs ( $37 \mu\text{s}$  and  $65 \mu\text{s}$ ). The black histograms and red crosses show the light curves and time-energy scatters, respectively. The vertical and horizontal for all TGFs are on the same scales except for (b) and (c).

249 **4 GECAM TEBs**

250 The GECAM CPDs are mostly used to detect electrons and positrons in orbit, while  
 251 it has low detection efficiency to gamma-ray (Xu et al., 2022). To distinguish between  
 252 TGFs and TEBs, we find a very effective threshold considering the duration and CPD/GRD  
 253 counts ratio (see Figure 3d).

254 In this paper, we present four high-confidence TEBs, as shown in Figure 2, Fig-  
 255 ure 3d, and Figure 5. Although TEBs can also produce many counts in GRDs, their du-  
 256 ration and the CPD/GRD counts ratio is remarkably different from TGFs. It is explic-  
 257 itly shown in Figure 3d that the TEBs and TGFs are separated into two groups accord-  
 258 ing to duration and CPD/GRD counts ratio. The CPD/GRD counts ratio for all TGFs  
 259 is  $< 0.25$  and mostly  $< 0.15$ , while that of TEBs reaches  $\sim 0.35$ . It should be noticed  
 260 that the negative values of the CPD/GRD counts ratio mean no significant signals reg-  
 261 istered in CPDs. The duration of TGFs ( $< 1$  ms) and TEBs ( $> 2$  ms) are also distinc-  
 262 tively different.

263 GECAM-B detected an interesting TEB event with two pulses separated by  $\sim 150$   
 264 ms (Figure 5a) that occurred over the Southwest Indian Ocean at 18:34:40.552 UTC on  
 265 September 11th, 2021. Unlike the bright main peak and weak return peak in a typical  
 266 TEB, these two pulses have similar brightness. Since TEB electrons will travel along the  
 267 Earth's magnetic field lines, we trace this line using the International Geomagnetic Ref-  
 268 erence Field (IGRF) 13 model (Alken et al., 2021). As shown in Figure 5e and 5f, there  
 269 is no lightning activity around the GECAM nadir ( $51.2^\circ$  E,  $28.9^\circ$  S, 587.7 km) and the  
 270 southern magnetic footpoint ( $-31.3^\circ$  E,  $52.8^\circ$  N, 40 km) within  $\pm 1$  minute of the TEB  
 271 time and a radius of 1200 km. However, there is a cluster of WWLLN lightning around  
 272 the northern magnetic footpoint ( $44.1^\circ$  E,  $45.5^\circ$  N, 40 km) within 400 km and  $\pm 10$  sec-  
 273 onds. Moreover, the expected round-trip bounce time between the GECAM-B satellite  
 274 and the southern footpoint is  $< \sim 17$  ms for 100 keV electrons, which is an order of mag-  
 275 nitude lower than the observed time interval between the two pulses, strongly disfavor-  
 276 ing the return peak nature of the second pulse.

277 Considering the lack of lightning discharge in the southern part and intense light-  
 278 ning activity in the northern part, as well as the expected time interval for TEB elec-  
 279 trons, bounce from GECAM and the southern footpoint is far less than 150 ms, it is highly  
 280 likely that the TEB electrons of both pulses originate from TGFs occurred around the  
 281 northern footpoint in the same lightning discharge process. Even if they are produced  
 282 by two TGF events, the distance between these two TGFs should not be very far, oth-  
 283 erwise, they would not be detected as TEB at the same location of GECAM-B. As far  
 284 as we are aware of, this TEB is the first reported event with two pulses that originate  
 285 from the same geomagnetic footpoint.

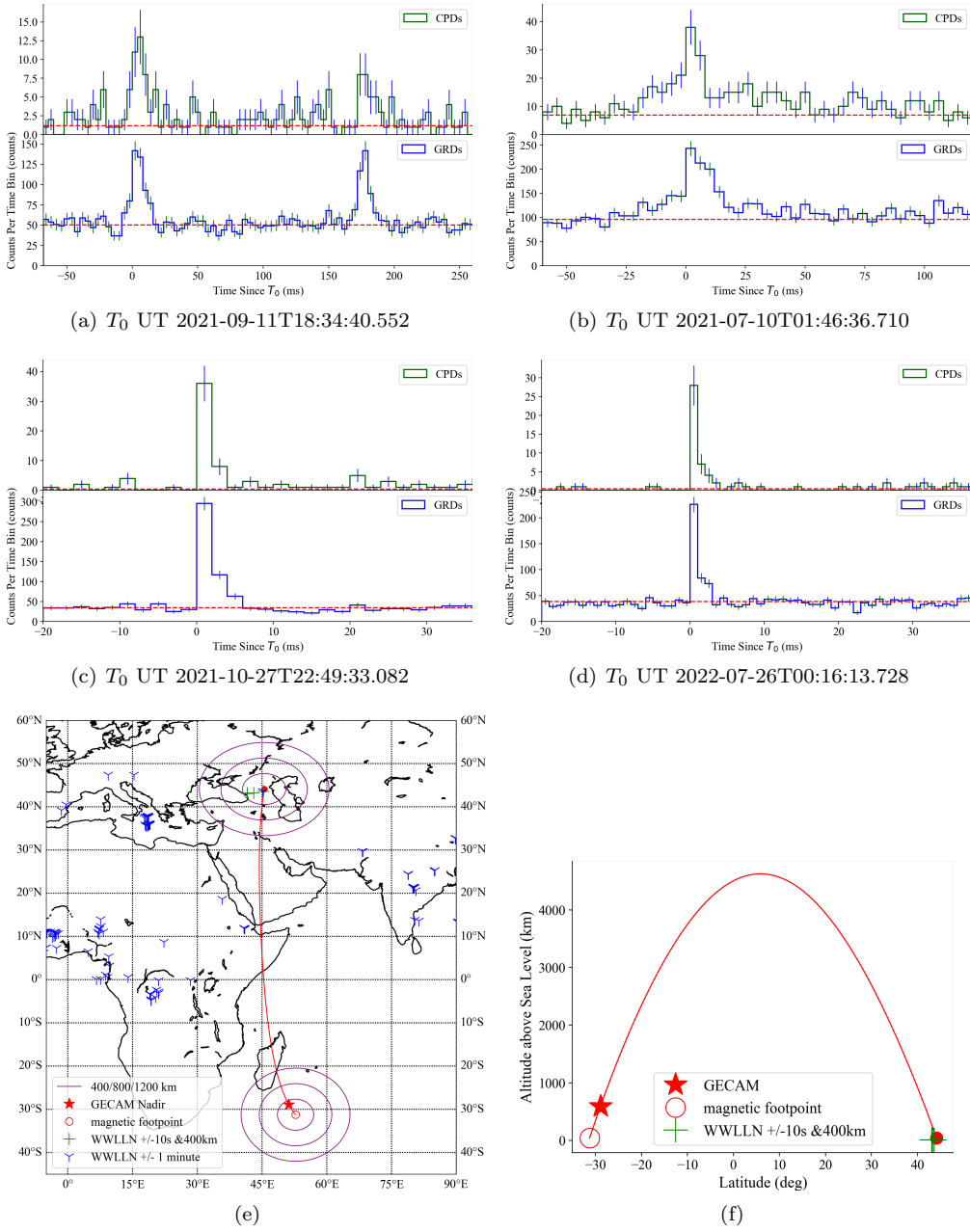


**Figure 5.** (a) to (d) The light curves of 4 GECAM TEBs. For each TEB, the upper and lower panels show the light curves of CPDs and GRDs, respectively. It should be noted that there are two pulses which episode by  $\sim 150$  ms on subfigure (a). (e) Map of GECAM nadir (red star), WWLLN lightning (blue triangles and green pluses), the traced magnetic field line (red line), and their footpoints (red circles) for the TEBs shown in subfigure (a). (f) The latitude-altitude projected map of the TEBs shown in subfigure (a). The blue triangles illustrate total WWLLN detections within 60 seconds, and green pluses illustrate the WWLLN lightning around the northern magnetic footpoint 400 km within 10 seconds. The solid red circle shows the northern magnetic footpoint and the hollow red circle shows the southern magnetic footpoint.

## 5 Conclusion

With novel designs on detectors and electronics, GECAM is a new powerful instrument to detect and identify TGFs and TEBs, as well as study their properties. Thanks to the high time resolution (100 ns), broad detection energy range (several keV to several MeV), and anti-saturation designs, GECAM can record very bright TGFs and TEBs, and reveal their fine structures in light curves and spectrum, which can help us better understand the production mechanism of TGFs and TEBs.

In this paper, a GECAM TGF/TEB search algorithm is proposed, then 147 bright TGFs and 4 TEBs are identified. The TGF detection rate for GECAM-B is  $\sim 200$  TGFs/year, which will increase if we loose the search threshold. The GECAM-GLD360 lightning-association ratio reaches  $\sim 80\%$  in the east Asia region, significantly higher than previous results obtained with the other space-borne instruments and the WWLLN data. A few interesting structures of TGFs are notable, such as a short spike (down to  $\sim 10 \mu\text{s}$ ) lying on the decay phase of the main pulse, an interesting double-peak TGF with very similar temporal and spectral distribution, and more than 40 counts are registered in an extremely short duration of  $\sim 37 \mu\text{s}$ .

For mostly gamma-ray space telescopes, determining a TEB is not straightforward, e.g. through the 511 keV line of the spectrum and the return peak. With the joint observation of GRDs and CPDs, GECAM can directly distinguish between TGFs and TEBs according to the duration distribution and CPD/GRD counts ratio. We find an interesting TEB with two pulses which probably originated from a special lightning discharge process.

## Acknowledgments

The GECAM (HuaiRou-1) mission is supported by the Strategic Priority Research Program on Space Science of the Chinese Academy of Sciences, China. This work is supported by the National Key R&D Program of China (2021YFA0718500). We thank the support from the Strategic Priority Research Program on Space Science, the Chinese Academy of Sciences (Grant No. XDA15360102, XDA15360300, XDA15052700), the National Natural Science Foundation of China (Grant No. 12273042, 12173038, 42274205, U1938115, U2038106), the National HEP Data Center (Grant No. E029S2S1) and the open fund of Hubei LuoJia Laboratory (Grant No. 220100051). We thank Xi Long (Harvard University) for the helpful discussions. The GLD360 data used in this paper belong to Vaisala Inc who supports the ASIM project. The authors wish to thank the World Wide Lightning Location Network (<http://wwlln.net>) as a collaboration of more than 50 universities.

## References

- Alken, P., Thébault, E., Beggan, C. D., Amit, H., Aubert, J., Baerenzung, J., ... others (2021). International geomagnetic reference field: the thirteenth generation. *Earth, Planets and Space*, *73*(1), 1–25.
- An, Z. H., Sun, X. L., Zhang, D. L., Yang, S., Li, X. Q., Wen, X. Y., ... Zhou, X. (2022). The design and performance of grd onboard the geom satellite [Journal Article]. *Radiation Detection Technology and Methods*, *6*(1), 43–52. Retrieved from <https://doi.org/10.1007/s41605-021-00289-y> doi: 10.1007/s41605-021-00289-y
- Briggs, M. S., Fishman, G., Connaughton, V., Bhat, P., Paciesas, W., Preece, R., ... others (2010). First results on terrestrial gamma ray flashes from the fermi gamma-ray burst monitor. *Journal of Geophysical Research: Space Physics*, *115*(A7).
- Briggs, M. S., Xiong, S., Connaughton, V., Tierney, D., Fitzpatrick, G., Foley, S., ... others (2013). Terrestrial gamma-ray flashes in the fermi era: Improved observations and analysis methods. *Journal of Geophysical Research: Space Physics*, *118*(6), 3805–3830.
- Cai, C., Xiong, S. L., Li, C. K., Liu, C. Z., Zhang, S. N., Li, X. B., ... Zhou, D. K. (2021, 09). Search for gamma-ray bursts and gravitational wave electromagnetic counterparts with High Energy X-ray Telescope of Insight-HXMT. *Monthly Notices of the Royal Astronomical Society*, *508*(3), 3910–3920. Retrieved from <https://doi.org/10.1093/mnras/stab2760> doi: 10.1093/mnras/stab2760
- Cai, C., Xiong, S.-L., Xue, W.-C., Zhao, Y., Xiao, S., Yi, Q.-B., ... Zhang, F. (2022, 10). Burst search method based on likelihood ratio in Poisson statistics. *Monthly Notices of the Royal Astronomical Society*, *518*(2), 2005–2014. Retrieved from <https://doi.org/10.1093/mnras/stac3075> doi: 10.1093/mnras/stac3075
- Celestin, S., & Pasko, V. P. (2011). Energy and fluxes of thermal runaway electrons produced by exponential growth of streamers during the stepping of lightning leaders and in transient luminous events. *Journal of Geophysical Research: Space Physics*, *116*(A3).
- Celestin, S., Xu, W., & Pasko, V. (2013). Spectra of x-ray and gamma-ray bursts produced by stepping lightning leaders. In *Egu general assembly conference abstracts* (p. 13065).
- Chanrion, O., & Neubert, T. (2010). Production of runaway electrons by negative streamer discharges. *Journal of Geophysical Research: Space Physics*, *115*(A6).
- Dwyer, J. (2003). A fundamental limit on electric fields in air. *Geophysical Research Letters*, *30*(20).
- Dwyer, J. (2008). Source mechanisms of terrestrial gamma-ray flashes. *Journal of Geophysical Research: Atmospheres*, *113*(D10).
- Dwyer, J. (2012). The relativistic feedback discharge model of terrestrial gamma ray flashes. *Journal of Geophysical Research: Space Physics*, *117*(A2).
- Dwyer, J. R. (2010). Diffusion of relativistic runaway electrons and implications for lightning initiation. *Journal of Geophysical Research: Space Physics*, *115*(A3).
- Dwyer, J. R., Grefenstette, B. W., & Smith, D. M. (2008). High-energy electron beams launched into space by thunderstorms. *Geophysical Research Letters*, *35*(2).
- Dwyer, J. R., Schaal, M. M., Cramer, E., Arabshahi, S., Liu, N., Rassoul, H., ... Uman, M. A. (2012). Observation of a gamma-ray flash at ground level in association with a cloud-to-ground lightning return stroke. *Journal of Geophysical Research: Space Physics*, *117*(A10).
- Dwyer, J. R., & Smith, D. M. (2005). A comparison between monte carlo simulations of runaway breakdown and terrestrial gamma-ray flash observations.

- 376 *Geophysical Research Letters*, 32(22).
- 377 Feng, H., Li, T., Wu, M., Zha, M., & Zhu, Q. (2002). Temporal and spectral proper-  
378 ties of gamma-ray flashes. *Geophysical research letters*, 29(3), 6–1.
- 379 Fishman, G. J., Bhat, P. N., Mallozzi, R., Horack, J. M., Koshut, T., Kouveliotou,  
380 C., ... Christian, H. J. (1994). Discovery of intense gamma-ray flashes of at-  
381 mospheric origin. *Science*, 264(5163), 1313–1316. Retrieved 2022-05-05, from  
382 <http://www.jstor.org/stable/2884079>
- 383 Goldstein, A., Veres, P., Burns, E., Briggs, M. S., Hamburg, R., Kocevski, D., ...  
384 Stanbro, M. (2017, oct). An ordinary short gamma-ray burst with extraor-  
385 dinary implications: Fermi-gbm detection of grb 170817a. *The Astrophysical*  
386 *Journal*, 848(2), L14. Retrieved from [https://doi.org/10.3847/2041-8213/](https://doi.org/10.3847/2041-8213/aa8f41)  
387 [aa8f41](https://doi.org/10.3847/2041-8213/aa8f41) doi: 10.3847/2041-8213/aa8f41
- 388 Grefenstette, B. W., Smith, D. M., Hazelton, B., & Lopez, L. (2009). First rhesi  
389 terrestrial gamma ray flash catalog. *Journal of Geophysical Research: Space*  
390 *Physics*, 114(A2).
- 391 Gurevich, A., Milikh, G., & Roussel-Dupre, R. (1992). Runaway electron mechanism  
392 of air breakdown and preconditioning during a thunderstorm. *Physics Letters*  
393 *A*, 165(5-6), 463–468.
- 394 Han, X., Zhang, K., Huang, J., YU, J., XIONG, S., CHEN, Y., ... GENG, H. (2020).  
395 Gecam satellite system design and technological characteristic [Journal Ar-  
396 ticle]. *SCIENTIA SINICA Physica, Mechanica & Astronomica*, 50(1674-  
397 7275), 129507. Retrieved from [https://www.sciengine.com/publisher/](https://www.sciengine.com/publisher/ScienceChinaPress/journal/SCIENTIASINICAPhysica,Mechanica&Astronomica/50/12/10.1360/SSPMA-2020-0120)  
398 [ScienceChinaPress/journal/SCIENTIASINICAPhysica,Mechanica\](https://www.sciengine.com/publisher/ScienceChinaPress/journal/SCIENTIASINICAPhysica,Mechanica&Astronomica/50/12/10.1360/SSPMA-2020-0120)  
399 [&Astronomica/50/12/10.1360/SSPMA-2020-0120](https://www.sciengine.com/publisher/ScienceChinaPress/journal/SCIENTIASINICAPhysica,Mechanica&Astronomica/50/12/10.1360/SSPMA-2020-0120) doi: [https://doi.org/](https://doi.org/10.1360/SSPMA-2020-0120)  
400 [10.1360/SSPMA-2020-0120](https://doi.org/10.1360/SSPMA-2020-0120)
- 401 Klebesadel, R. W., Strong, I. B., & Olson, R. A. (1973). Observations of gamma-ray  
402 bursts of cosmic origin. *The Astrophysical Journal*, 182, L85.
- 403 Li, et al. (2022). The technology for detection of gamma-ray burst with GECAM  
404 satellite. *Radiation Detection Technology and Methods*. doi: 10.1007/s41605-  
405 -021-00288-z
- 406 Lindanger, A., Marisaldi, M., Maiorana, C., Sarria, D., Albrechtsen, K., Østgaard,  
407 N., ... others (2020). The 3rd agile terrestrial gamma ray flash catalog. part i:  
408 Association to lightning sferics. *Journal of Geophysical Research: Atmospheres*,  
409 125(11), e2019JD031985.
- 410 Liu, N., & Dwyer, J. R. (2013). Modeling terrestrial gamma ray flashes produced  
411 by relativistic feedback discharges. *Journal of Geophysical Research: Space*  
412 *Physics*, 118(5), 2359–2376.
- 413 Liu, Y., Gong, K., Li, X., Wen, X., An, Z., Cai, C., ... others (2021). The sipm  
414 array data acquisition algorithm applied to the gecam satellite payload. *arXiv*  
415 *preprint arXiv:2112.04786*.
- 416 Lorimer, D. R., Bailes, M., McLaughlin, M. A., Narkevic, D. J., & Crawford, F.  
417 (2007). A bright millisecond radio burst of extragalactic origin. *Science*,  
418 318(5851), 777–780.
- 419 Lu, G., Blakeslee, R. J., Li, J., Smith, D. M., Shao, X.-M., McCaul, E. W., ... Cum-  
420 mer, S. A. (2010). Lightning mapping observation of a terrestrial gamma-ray  
421 flash. *Geophysical Research Letters*, 37(11).
- 422 Lu, G., Cummer, S. A., Li, J., Han, F., Smith, D. M., & Grefenstette, B. W. (2011).  
423 Characteristics of broadband lightning emissions associated with terrestrial  
424 gamma ray flashes. *Journal of Geophysical Research: Space Physics*, 116(A3).
- 425 Lyu, F., Cummer, S. A., Lu, G., Zhou, X., & Weinert, J. (2016). Imaging lightning  
426 intracloud initial stepped leaders by low-frequency interferometric lightning  
427 mapping array. *Geophysical Research Letters*, 43(10), 5516–5523.
- 428 Maiorana, C., Marisaldi, M., Lindanger, A., Østgaard, N., Ursi, A., Sarria, D., ...  
429 others (2020). The 3rd agile terrestrial gamma-ray flashes catalog. part ii:  
430 Optimized selection criteria and characteristics of the new sample. *Journal of*

- 431 *Geophysical Research: Atmospheres*, 125(11), e2019JD031986.
- 432 Marisaldi, M., Fuschino, F., Labanti, C., Galli, M., Longo, F., Del Monte, E., ... oth-  
 433 ers (2010). Detection of terrestrial gamma ray flashes up to 40 mev by the  
 434 agile satellite. *Journal of Geophysical Research: Space Physics*, 115(A3).
- 435 Marisaldi, M., Galli, M., Labanti, C., Østgaard, N., Sarria, D., Cummer, S., ... others  
 436 (2019). On the high-energy spectral component and fine time structure of  
 437 terrestrial gamma ray flashes. *Journal of Geophysical Research: Atmospheres*,  
 438 124(14), 7484–7497.
- 439 Mezentsev, A., Østgaard, N., Gjesteland, T., Albrechtsen, K., Lehtinen, N.,  
 440 Marisaldi, M., ... Cummer, S. (2016). Radio emissions from double rhesi  
 441 tgfs. *Journal of Geophysical Research: Atmospheres*, 121(13), 8006–8022.
- 442 Moss, G. D., Pasko, V. P., Liu, N., & Veronis, G. (2006). Monte carlo model for  
 443 analysis of thermal runaway electrons in streamer tips in transient luminous  
 444 events and streamer zones of lightning leaders. *Journal of Geophysical Re-*  
 445 *search: Space Physics*, 111(A2).
- 446 Nemiroff, R. J., Bonnell, J. T., & Norris, J. P. (1997). Temporal and spectral char-  
 447 acteristics of terrestrial gamma flashes. *Journal of Geophysical Research: Space*  
 448 *Physics*, 102(A5), 9659–9665.
- 449 Østgaard, N., Neubert, T., Reglero, V., Ullaland, K., Yang, S., Genov, G., ... others  
 450 (2019). First 10 months of tgf observations by asim. *Journal of Geophysical*  
 451 *Research: Atmospheres*, 124(24), 14024–14036.
- 452 Poelman, D. R., Schulz, W., & Vergeiner, C. (2013). Performance characteristics of  
 453 distinct lightning detection networks covering belgium. *Journal of Atmospheric*  
 454 *and Oceanic Technology*, 30(5), 942–951.
- 455 Pohjola, H., & Mäkelä, A. (2013). The comparison of gld360 and euclid lightning lo-  
 456 cation systems in europe. *Atmospheric research*, 123, 117–128.
- 457 Roberts, O. J., Fitzpatrick, G., Stanbro, M., McBreen, S., Briggs, M. S., Holzworth,  
 458 R. H., ... Mailyan, B. G. (2018). The first fermi-gbm terrestrial gamma ray  
 459 flash catalog. *Journal of Geophysical Research: Space Physics*, 123(5), 4381-  
 460 4401. Retrieved from [https://agupubs.onlinelibrary.wiley.com/doi/abs/](https://agupubs.onlinelibrary.wiley.com/doi/abs/10.1029/2017JA024837)  
 461 [10.1029/2017JA024837](https://doi.org/10.1029/2017JA024837) doi: <https://doi.org/10.1029/2017JA024837>
- 462 Said, R., Cohen, M., & Inan, U. (2013). Highly intense lightning over the oceans:  
 463 Estimated peak currents from global gld360 observations. *Journal of Geophysi-*  
 464 *cal Research: Atmospheres*, 118(13), 6905–6915.
- 465 Sarria, D., Østgaard, N., Kochkin, P., Lehtinen, N., Mezentsev, A., Marisaldi, M.,  
 466 ... others (2021). Constraining spectral models of a terrestrial gamma-ray  
 467 flash from a terrestrial electron beam observation by the atmosphere-space  
 468 interactions monitor. *Geophysical Research Letters*, 48(9), e2021GL093152.
- 469 Scargle, J. D., Norris, J. P., Jackson, B., & Chiang, J. (2013, feb). Studies in  
 470 astronomical time series analysis. vi. bayesian block representations. *The As-*  
 471 *trophysical Journal*, 764(2), 167. Retrieved from [https://doi.org/10.1088/](https://doi.org/10.1088/0004-637x/764/2/167)  
 472 [0004-637x/764/2/167](https://doi.org/10.1088/0004-637x/764/2/167) doi: [10.1088/0004-637x/764/2/167](https://doi.org/10.1088/0004-637x/764/2/167)
- 473 Skeltved, A. B., Østgaard, N., Mezentsev, A., Lehtinen, N., & Carlson, B. (2017).  
 474 Constraints to do realistic modeling of the electric field ahead of the tip of  
 475 a lightning leader. *Journal of Geophysical Research: Atmospheres*, 122(15),  
 476 8120–8134.
- 477 Stolzenburg, M., Marshall, T. C., Karunarathne, S., & Orville, R. E. (2016). Lumi-  
 478 nosity with intracloud-type lightning initial breakdown pulses and terrestrial  
 479 gamma-ray flash candidates. *Journal of Geophysical Research: Atmospheres*,  
 480 121(18), 10–919.
- 481 Ursi, A., Guidorzi, C., Marisaldi, M., Sarria, D., & Frontera, F. (2017). Terrestrial  
 482 gamma-ray flashes in the beposax data archive. *Journal of Atmospheric and*  
 483 *Solar-Terrestrial Physics*, 156, 50–56.
- 484 Wilson, C. T. (1925). The acceleration of  $\beta$ -particles in strong electric fields such  
 485 as those of thunderclouds. In *Mathematical proceedings of the cambridge philo-*

- 486 *sophical society* (Vol. 22, pp. 534–538).
- 487 Woods, P., & Thompson, C. (2004). Soft gamma repeaters and anomalous x-ray  
488 pulsars: magnetar candidates. *arXiv preprint astro-ph/0406133*.
- 489 Xiao, S., Liu, Y., Peng, W., An, Z., Xiong, S., Tuo, Y., ... others (2022). On-ground  
490 and on-orbit time calibrations of gecam. *Monthly Notices of the Royal Astro-*  
491 *nomical Society*, 511(1), 964–971.
- 492 Xiong, S., Briggs, M., Connaughton, V., Fishman, G., Tierney, D., Fitzpatrick,  
493 G., ... Hutchins, M. (2012). Location prediction of electron tgfs. *Journal of*  
494 *Geophysical Research: Space Physics*, 117(A2).
- 495 Xu, W., Celestin, S., & Pasko, V. P. (2012). Source altitudes of terrestrial gamma-  
496 ray flashes produced by lightning leaders. *Geophysical Research Letters*, 39(8).
- 497 Xu, W., Celestin, S., & Pasko, V. P. (2015). Optical emissions associated with  
498 terrestrial gamma ray flashes. *Journal of Geophysical Research: Space Physics*,  
499 120(2), 1355–1370.
- 500 Xu, Y. B., Li, X. Q., Sun, X. L., Yang, S., Wang, H., Peng, W. X., ... Zhou, X.  
501 (2022). The design and performance of charged particle detector onboard the  
502 gecam mission [Journal Article]. *Radiation Detection Technology and Methods*,  
503 6(1), 53-62. Retrieved from <https://doi.org/10.1007/s41605-021-00298-x>  
504 doi: 10.1007/s41605-021-00298-x
- 505 Zhang, et al. (2022). Dedicated sipm array for grd of gecam. *Radiation Detection*  
506 *Technology and Methods*, 6(1), 63–69.
- 507 Zhao, X., Xiong, S., Wen, X., Li, X., Cai, C., Xiao, S., & Luo, Q. (2021, December).  
508 The In-Flight Realtime Trigger and Localization Software of GECAM. *arXiv*  
509 *e-prints*, arXiv:2112.05101.
- 510 Zhao, Y., Xue, W., Xiong, S., Luo, Q., YQ, Z., H, Y., ... SN, Z. (2022, September).  
511 On the Localization Methods of High Energy Transients for All-Sky Gamma-  
512 Ray Monitors. *arXiv e-prints*, arXiv:2209.13088.
- 513 Zhao, Y., Xue, W., Xiong, S., Wang, Y., Liu, J., Luo, Q., ... Yu, H. (2022, Novem-  
514 ber). GECAM Localization of High Energy Transients and the Systematic Er-  
515 ror. *arXiv e-prints*, arXiv:2211.15570.